CHAPTER

11 Computed Tomography and Magnetic Resonance Imaging

Kyongtae T. Bae • Sonal Krishan

Cross-sectional imaging is essential for the diagnosis and clinical management of a number of renal pathologies. Although ultrasound (US) represents a first-line imaging modality in the assessment of the kidney because of its cost effectiveness, portability, and availability, the images are highly operator dependent and are limited in anatomic coverage as compared to computed tomography (CT) scans and magnetic resonance imaging (MRI). CT scans and MRIs offer images of superb anatomic detail and permit the accurate and noninvasive assessment of a wide range of renal and urologic pathologies including: congenital anomalies, obstructive disease, inflammatory lesions, vascular insufficiency, benign and malignant tumors, and trauma. Although CT scans remain far more commonly used in clinical settings, the role of MRI is growing because of its superior intrinsic tissue contrast and the absence of radiation exposure. Additionally, MRIs can be used as the problem-solving modality when US or CT findings are nondiagnostic.

TECHNICAL CONSIDERATIONS FOR COMPUTED TOMOGRAPHY SCANS AND MAGNETIC RESONANCE IMAGING

Principles of Computed Tomography Scans

Similar to conventional X-ray radiographic images, the physical basis for a CT scan is the attenuation of X-ray photons passing through the body. The basic hardware of a CT scanner system consists of an X-ray gantry (which supports a rotating X-ray tube and a set of X-ray detectors); a patient table that moves in and out of the gantry; and a computer system integrated with the gantry, data-storage hardware, and image-display console. A precisely collimated narrow X-ray beam (a fan-shaped beam) is generated, then transmitted through the patient's body and received and identified by the detectors on the opposite side of the gantry. The use of a rotating X-ray beam and detector arrays permits the detection and measurement of the X-rays attenuated by tissues from many different projections. It is from these measurements that the CT images are mathematically reconstructed.[1] The CT scan is operated at various user-selectable voltages (e.g., 80, 100, 120, 140 kVp) and currents (milliampere second [mAs]) that closely determine radiation dose and image quality.

Computed Tomography Attenuation or Computed Tomography Number (Hounsfield unit)

The spatial resolution of a CT image typically achieves 0.3 to 0.5 mm with an imaging matrix size of 512 × 512 pixels. Each pixel (picture element) value of a CT image represents the tissues' X-ray attenuation coefficient at that pixel, which is expressed in Hounsfield units (HU). The data size of each pixel is typically 2 bytes. Because a CT image consists of 512 × 512 pixels, the data size of a CT image is approximately 0.5 MB (512 × 512 × 2). The attenuation value assigned to each pixel is based on a reference scale in which −1,000 HU is the value assigned to air and 0 HU is assigned to water.[2] Fat is typically −30 HU or less, whereas calcification, bone, and iodinated contrast are usually greater than 100 HU. User selection of the number of shades of gray (window width) in the image and the central hue of gray (window level) permits the modification of displayed image contrast. By adjusting the window width and level, the image can be optimized for evaluating a wide range of tissues with varying attenuations. For example, bone and a contrast-filled bladder are typically presented as bright (high attenuation) structures, whereas the lungs are typically presented as dark (low attenuation) structures. Subtle structures such as a solid tumor within a normal parenchyma may be displayed more conspicuously in a specifically designed window setting (e.g., liver window).

Computed Tomography Technical Advances

CT technology has advanced from the traditional single-row detector array to a multiple-row detector array. Multidetector-row CT (MDCT) scans, which are now the standard method for performing CT examinations, allow

multiple channels of data to be acquired simultaneously. As a result, MDCT scans covers a large volume of area in a short scan time with thinner slices and an improved spatial resolution along the patient's craniocaudal axis. Presently, 64-detector MDCT systems are most commonly in use; however, the 320-detector MDCT has been recently introduced into clinical practice. Using MDCT, the entire abdomen can be imaged in a few seconds. MDCT scans offer a greater speed of acquisition and higher resolution images than single-detector CT scans and thus greatly facilitate multiplanar imaging and three-dimensional (3D) reconstruction (Fig. 11.1).

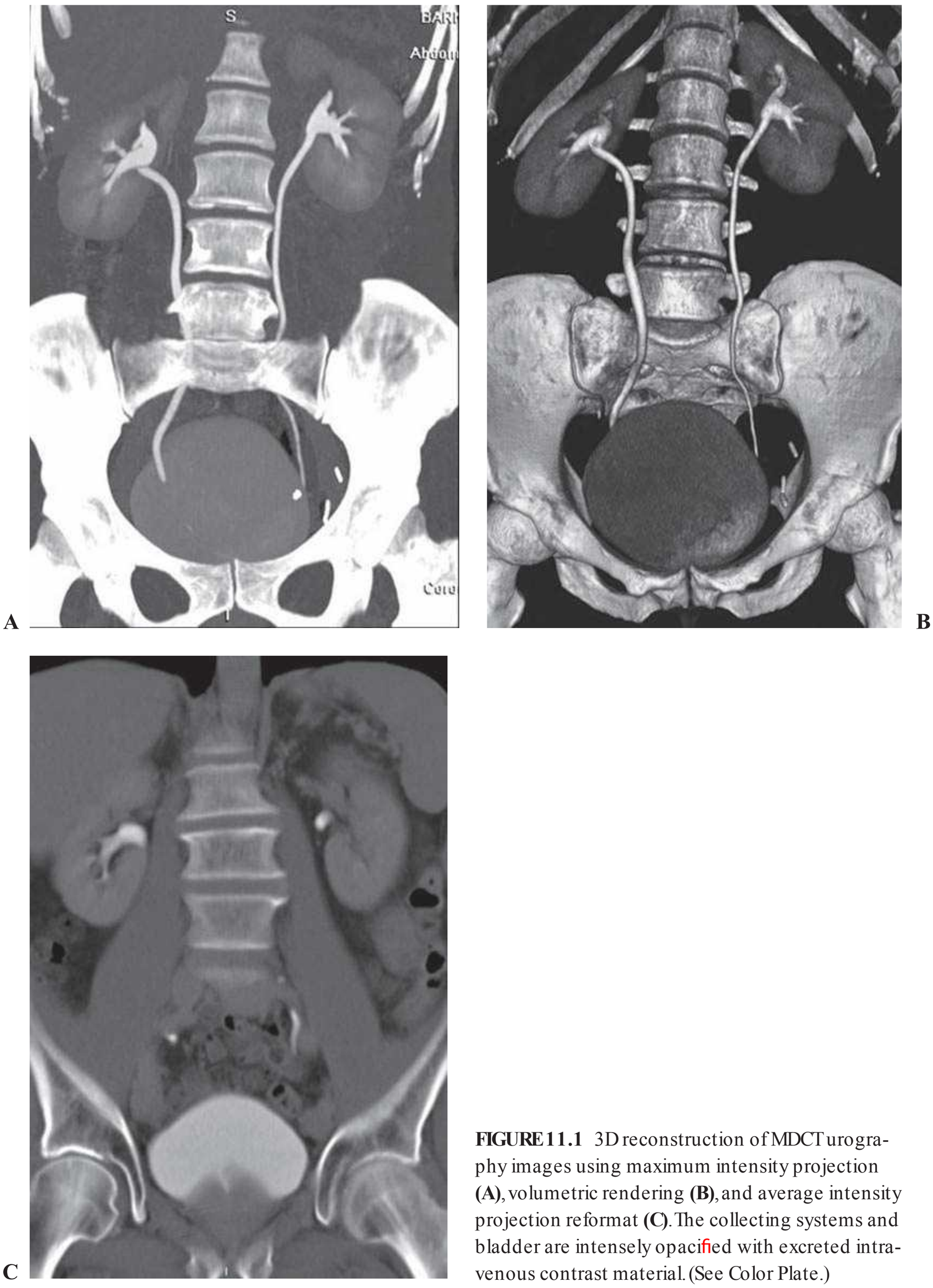

FIGURE 11.1 3D reconstruction of MDCT urography images using maximum intensity projection **(A)**, volumetric rendering **(B)**, and average intensity projection reformat **(C)**. The collecting systems and bladder are intensely opacified with excreted intravenous contrast material. (See Color Plate.)

The technical advances of MDCT scans have allowed highly technical and challenging clinical applications, such as CT angiography (CTA), to be practiced routinely. MDCT scans have essentially replaced the conventional catheter-based diagnostic renal angiography. In many institutions, MDCT urography is performed in place of the conventional intravenous urography.[3–5] MDCT renal imaging is widely used as the "one-stop shop" single imaging modality for the evaluation and surgical planning of many clinical conditions involving the kidney and urinary tract. In addition, the application of 3D techniques to CT scans allows for the accurate depiction of tumor depth, location, relationship of the tumor to adjacent structures, and the delineation of renal vascular anatomy as well as aid in preoperative planning (Fig. 11.2).

Recently, dual-energy MDCT scans were introduced, allowing the simultaneous acquisition of low- and high-voltage CT images during the same scanning phase. This technique has the potential to better characterize renal stone compositions and renal lesions through the assessment of their distinct CT attenuation profiles, thereby providing potentially improved physiologic and molecular information.[6]

Use of Contrast Media in Computed Tomography Scans

A CT evaluation of renal anatomy and pathology often requires the intravenous injection of iodinated contrast media. Intravenous contrast enhancement is useful for the depiction of small lesions by increasing their conspicuity, for the demonstration of vascular anatomy and vessel patency, and for the characterization of lesions through their patterns of contrast enhancement. On the other hand, an unenhanced CT scan is better suited to detect renal or urinary calcifications and intrarenal or perirenal hemorrhage because CT images obtained after the administration of contrast media may mask these abnormalities.[7–9] Unenhanced CT scans are also recommended for the quantification of tumor contrast enhancement on the postcontrast scans and for patients with poor renal function.

The commercially available radiographic contrast agents are tri-iodinated derivatives of benzoic acid. All currently available intravenous (IV) contrast media are excreted by the kidney through glomerular filtration, with no significant tubular excretion or resorption.[10,11] It is prudent that the physician inquire about the patient's history, particularly regarding the renal function and any history of allergies to the contrast material. A history of asthma and severe allergies increases the risk of subsequent reaction to contrast agent injection by a small percentage. The administration of corticosteroids, with or without antihistamines, 12 hours before a contrast injection to reduce the occurrence of adverse reactions in allergic patients has been well documented. Oral contrast is less critical in urologic imaging than in gastrointestinal imaging. In fact, the use of oral contrast media may be counterproductive for the evaluation of renal calculi or CTA.

A contrast-enhanced CT scan is typically performed with 100 to 150 mL of 300 to 370 mg per milliliter of contrast medium injected at 2 to 3 mL per second. The amount of contrast medium is adjusted for the patient's size, clinical indications, and the CT scanner type. For CTA, fast injection rates (4 to 5 mL per second) are recommended. CT scan delays are determined by fixed delay or bolus tracking techniques.[12]

After the administration of an IV contrast agent, contrast-enhanced CT scans can be acquired at different contrast enhancement phases: early arterial, corticomedullary, nephrographic, and excretory phases (in the order of increasing CT scan delays) (Fig. 11.3). Although the kidney is normally imaged in routine abdominal CT scans at a single (nephrographic) phase of contrast enhancement, dedicated renal imaging protocols consist of scanning of the kidney at multiphases of contrast enhancement. Imaging phases must be selected in accordance with clinical indications because it is important to minimize the number of scanning phases to reduce the radiation exposure for a patient.

The early arterial phase begins with the arrival of the contrast medium in the renal artery and ends prior to the occurrence of intense renal venous return. This phase is primarily useful in arterial CTA (i.e., surgical planning and renal artery stenosis evaluation) and is very limited for the diagnostic imaging of the kidney and urinary tract. The corticomedullary phase of the kidney corresponds to an intense enhancement of the renal cortex prior to a substantial enhancement in the medulla. The depiction of a hypervascular renal mass and renal artery anatomy is maximized during the corticomedullary phase. The nephrographic phase of the kidney corresponds to homogeneous enhancement throughout the renal parenchyma with a loss of corticomedullary differentiation. The depiction of renal lesions in the cortex or medulla is maximized during this phase. The degree of contrast enhancement in a renal mass is evaluated by noting the difference in the CT scan attenuation of the mass between this phase and in the unenhanced CT images. The onset of the excretory or urographic phase is about 2 minutes after the start of contrast medium injection. Maximal opacification of the renal calyces, pelvises, and ureters occurs later, about 5 to 10 minutes after the injection of the contrast medium. This is the best enhancement phase for the assessment of (benign and malignant) conditions affecting the urinary tract.

Magnetic Resonance Imaging Principles

An MRI scan begins with placing the patient in the central bore of an electromagnet, which generates a static magnetic field. Nuclei with odd numbers of protons or neutrons (of which hydrogen is the most abundant in biologic tissue) align themselves with their magnetic moments, either parallel or antiparallel to the external field. A net magnetization vector lies in a direction parallel to the static magnetic field of the magnet bore of the MRI (called the z-axis by convention). A radio frequency (RF) transmission coil transmits RF pulses through the patient and energizes the protons in the z-axis. When the RF pulse is turned off, the protons give off

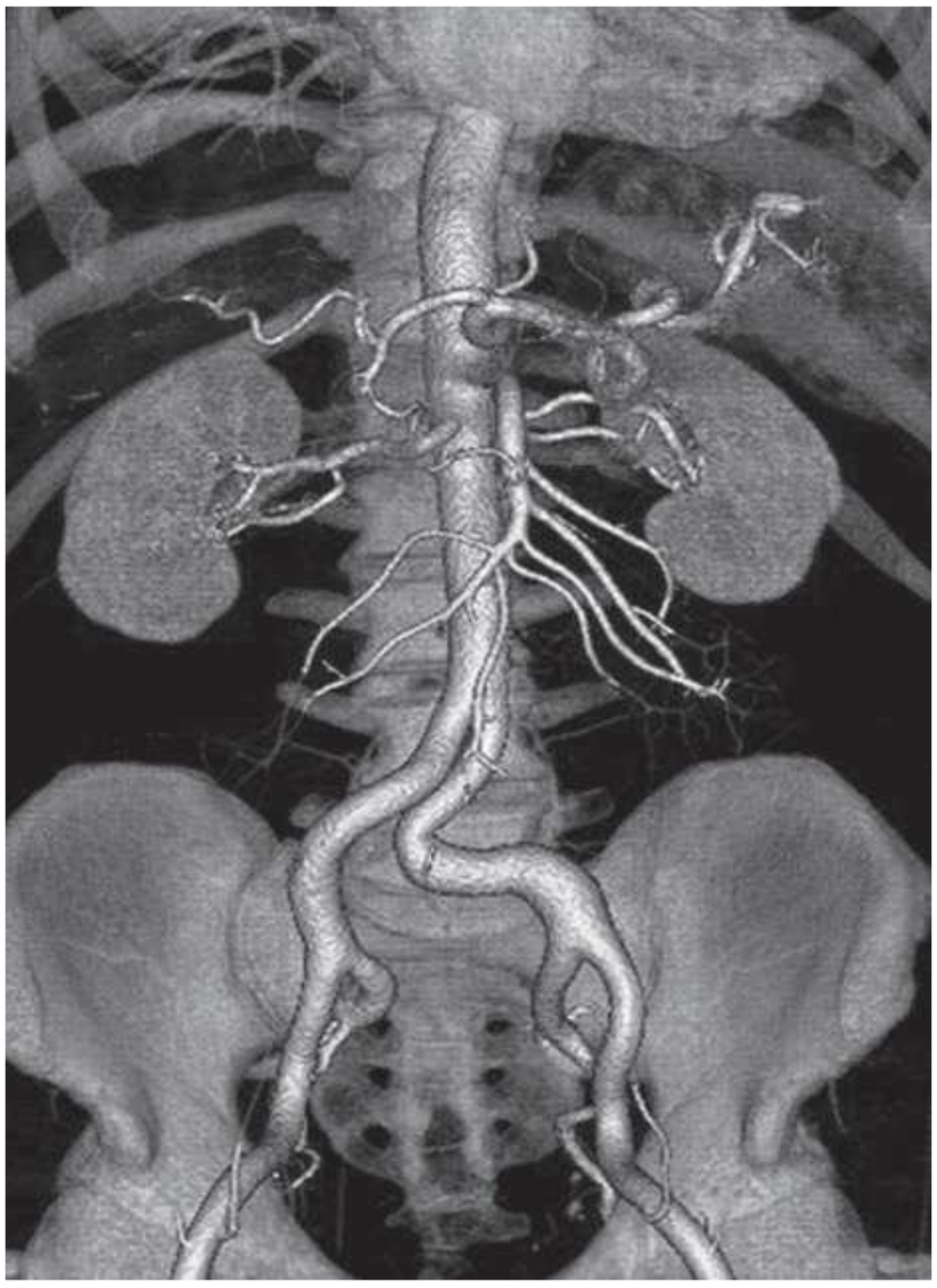

A

B

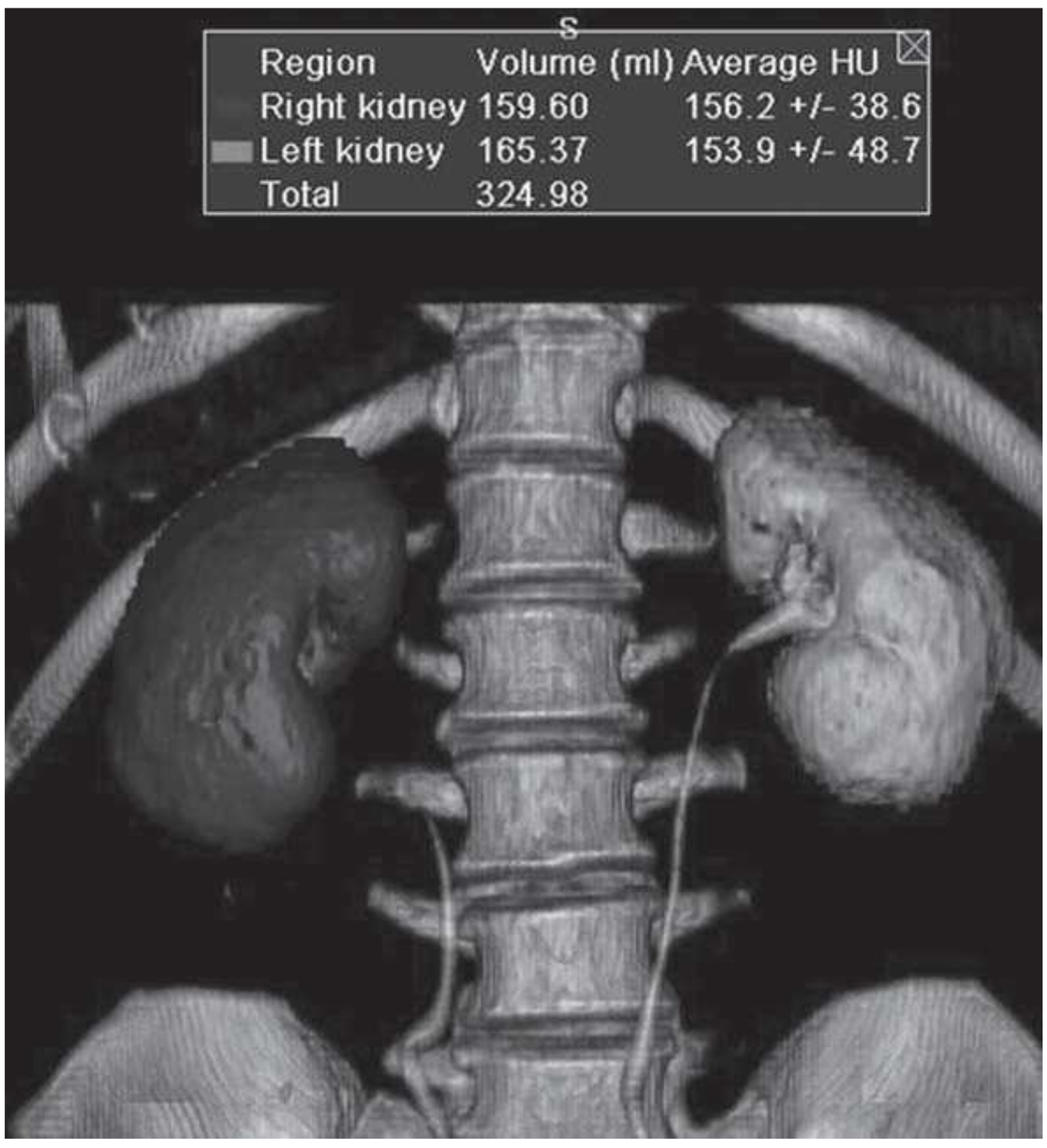

C

FIGURE 11.2 MDCT renal imaging performed as one-stop shop imaging study for renal donor work-up, including CT angiography **(A)**, urography **(B)**, and measurement of kidney volumes **(C)**. (See Color Plate.)

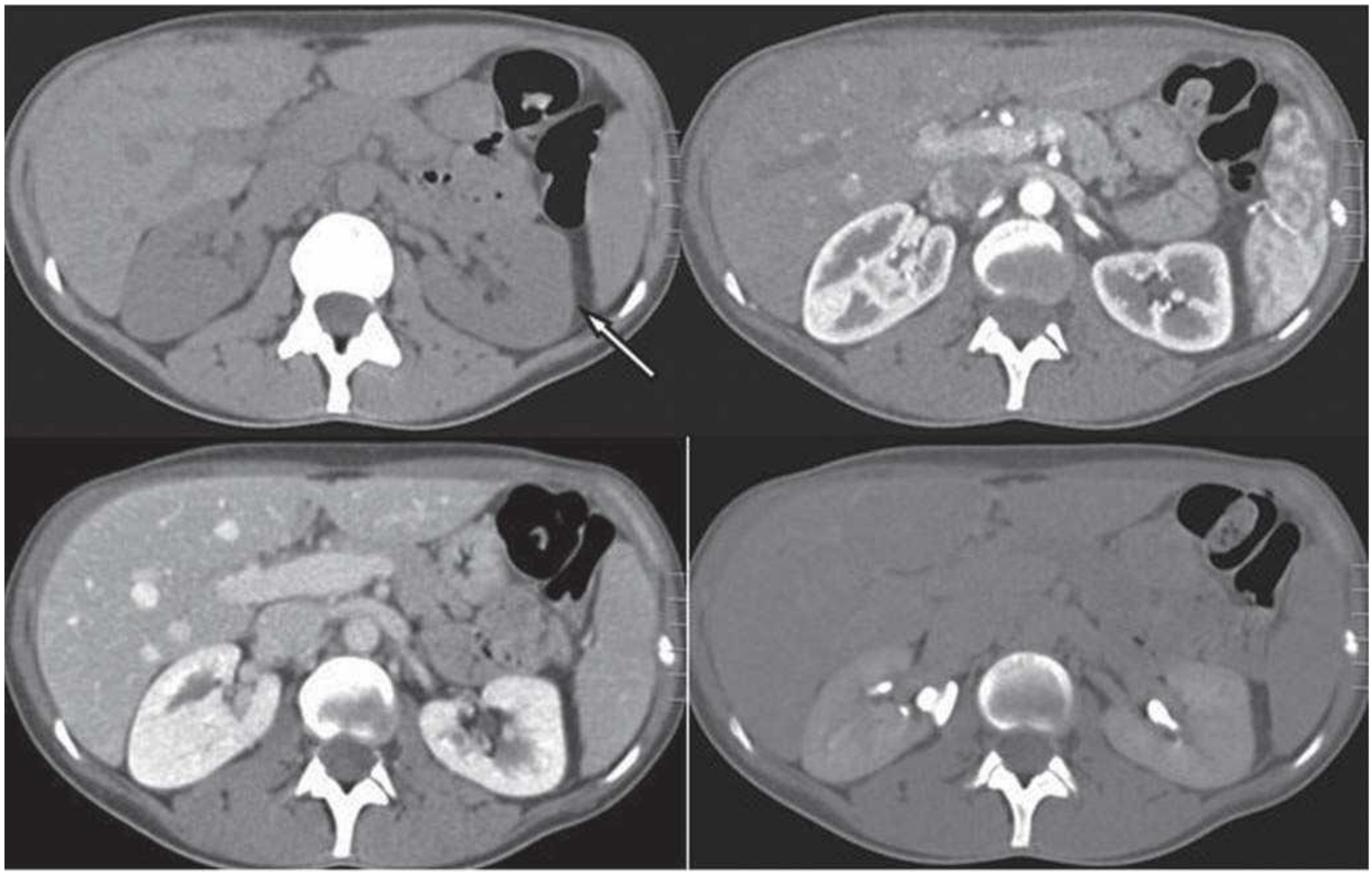

FIGURE 11.3 CT images of normal kidneys obtained without intravenous contrast (*left upper*), at corticomedullary phase with contrast (*right upper*), nephrographic phase (*left lower*), and delayed excretory phase (*right lower*). The arrow points to the peri-renal fat.

the energy (relaxation) that was imparted to them by the RF pulse.[13,14] This emitted energy is received by a receiver RF coil, and it is from this energy that the MR image is created. MRI pulse sequences determine the patterns of repetitive RF pulsations and the sampling of MR signals emitted during the intervals between RF pulses. Each MR sequence takes advantage of the intrinsic property of the body's tissues to absorb and release this energy. How this energy is imparted through the physics of the pulse sequences and whether energy is released quickly or slowly determines the weighting of an image. In general, an image is either T1 or T2 weighted. An MRI possesses exquisite contrast resolution, even without the use of IV contrast. On T1-weighted images, the fluid is generally dark (also called low signal) and on T2-weighted images, the fluid is bright (also called high signal).[13,14]

In order to map the anatomic distribution of different tissue signals, magnetic field gradients are established within the MR scanner along the x-, y-, and z-axes. Because the protons' resonance frequency depends on the magnetic field strength, controlled applications of magnetic field gradients induce protons to precess at different frequencies and phases according to their spatial distributions. The pattern of a received signal from a selected tissue volume can be converted to an image in which digital information related to protons' spatial distribution is reconstructed into images displayed over a gray scale.[13,14] Unlike CT attenuation values (HU), MR signal intensities are not directly specific to tissue compositions. Therefore, MR signal intensities between tissues are frequently compared in relative scales, such as a ratio to reference signal intensity.

Technical Advances in Magnetic Resonance Imaging

Because the respiratory motion of the kidney may significantly decrease the image quality, it is critical to perform an MRI scan with fast sequences within a breath hold. A variety of fast T1-weighted and T2-weighted sequences are available with the development of advanced coil and parallel imaging techniques to improve both temporal and spatial resolutions of an MRI. An MR angiography (MRA) is routinely performed when a diagnostic evaluation of the renal vasculature is requested. Although noncontrast sequences are available for an MRA, the dominant technique is the 3D gadolinium-enhanced MRA. For an evaluation of the urinary tract, an MR urography (MRU) has been developed. An MRU may be performed on T2-weighted sequences, exploiting the

long T2 of urine without gadolinium or on T1-weighted sequences after the administration of gadolinium contrast during the excretory phase.

Recent advances have resulted in new MR techniques for evaluating renal function such as perfusion, diffusion, oxygenation, and sodium concentration. A functional MRI of the kidney has not yet found broad clinical application, but it has great potential. Through the ongoing development of functional MRI techniques, we may expect an increasing role for functional MRIs in the management of patients with renal disease.[9,15,16]

The Use of Contrast Media in Magnetic Resonance Imaging

Gadolinium chelates are almost exclusively used for IV contrast materials for MRIs. Gadolinium agents have been shown to produce comparably lower incidences of allergic reactions than the iodinated contrast agents used in CT scans. The gadolinium compounds are filtered at the glomerulus and are neither reabsorbed nor secreted. They parallel iodinated contrast material in their pattern of initial intravascular and subsequent extracellular space distribution and in their pattern of excretion. Gadolinium-based contrast agents demonstrate a similar pattern of contrast enhancement as iodine-based agents (see Fig 11.4).[17,18]

For many years, gadolinium-based contrast-enhanced MRIs were believed to be safer and they were the preferred method of contrast (instead of iodine-based contrast material) for patients with renal impairments. However, since early 2006, evidence has been mounting that some gadolinium-based contrast agents may potentially cause the fibrosing sclerodermalike condition called nephrogenic systemic fibrosis (NSF) in patients with renal failure.[19–21] Patients at the highest risk of NSF include: (1) patients who have severe acute or chronic renal impairment with glomerular

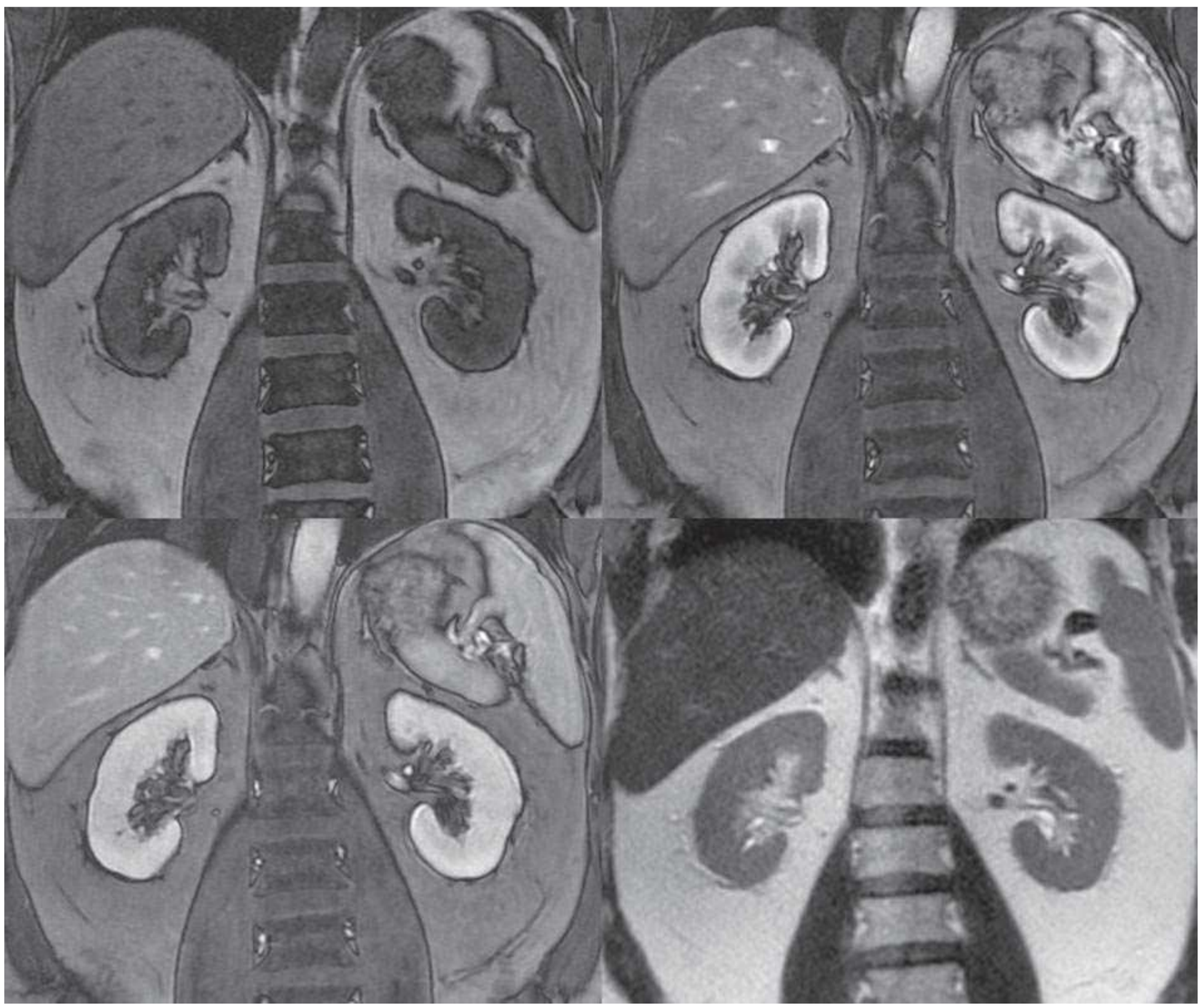

FIGURE 11.4 MR images of normal kidneys: T1-weighted without intravenous contrast (*left upper*), contrast-enhanced T1-weighted at corticomedullary phase (*right upper*), contrast-enhanced T1-weighted at nephrographic phase (*left lower*), and T2-weighted (*right lower*).

filtration rates (GFR) <30 mL per min/1.73m^2; (2) patients on dialysis (hemo or peritoneal); and (3) patients with reduced renal function awaiting liver transplantation. The recognition of this adverse reaction to gadolinium-based agents in renal-impaired patients emphasizes the need for an appropriate clinical indication for gadolinium-enhanced MRIs in this patient population. If an MRI is clearly indicated, the lowest dose of the agent that leaves the smallest amount of gadolinium in the body must be used and, in certain cases, immediate dialysis after the administration is recommended.[19–21]

MAGNETIC RESONANCE IMAGING VERSUS COMPUTED TOMOGRAPHY SCANS

CT scans and MRIs complement each other in providing diagnostic information for the detection and characterization of renal pathologies. Because CT scans are faster and easier to perform, it is more commonly used in the evaluation of renal and perirenal disease. The MRI remains primarily a problem solving modality adjunct to a CT scan or is used when a CT scan is contraindicated. The CT scan is superior for the reliable detection of calcified structures, whereas an MRI provides superb intrinsic tissue-contrast resolution and multiplanar imaging, which is particularly useful for the evaluation of renal vasculature.

If nephron sparing surgery is contemplated, an MRI is better able to differentiate a tumor from perinephric fat, the renal sinus, and the collecting system, thus helping the urologist decide if a partial nephrectomy is feasible. Staging renal lesions is more complete with an MRI than a CT scan, particularly when determining renal vein and inferior vena cava (IVC) involvement.[22,23] Patients who have genetic anomalies resulting in an increased risk for renal cell carcinoma (RCC) (e.g., von Hippel-Lindau), and those with conditions that produce other renal lesions that may mimic RCC (e.g., tuberous sclerosis), can be followed safely with a yearly MRI. This follow-up regimen will protect these high-risk patients from recurrent exposure to ionizing radiation from CT scans, with no loss in the ability to detect or characterize renal lesions.[24–37] Conversely, patients who are critically ill (e.g., intensive care unit patients) and those who have difficulty with the breath-holding requirements are not ideal candidates for renal MRIs. Patients unable to cooperate for other reasons (e.g., dementia, chronic obstructive pulmonary disease, morbidly obese) are also unsuitable for MRIs. Scanning these patients often results in a poor quality examination that may not be interpretable. Patients who have ferromagnetic implants (some neurovascular aneurysm clips, cochlear implants, pacemakers, defibrillators) are also contraindicated for MRIs. Furthermore, patients with claustrophobia may not be able to undergo MRIs.[24–37]

NORMAL ANATOMY

The kidneys lie within the retroperitoneum that is in turn divided by facial planes into three compartments centering the kidneys: the perirenal, the anterior pararenal, and the posterior pararenal spaces. The kidneys, the perirenal fat, and the adrenal gland are in the perirenal space enclosed by the anterior (Gerota) and posterior (Zuckerkandl) layers of the renal fascia. The perirenal space also includes the renal and adrenal vessels, the aorta, the inferior vena cava, and the perivascular lymph nodes. The kidneys lie lateral to and roughly parallel with the lateral border of the psoas muscle. The renal fossa is bounded medially by the psoas muscle, posteriorly by the quadratus lumborum muscle, laterally by the transversus abdominis muscles, and superiorly by the diaphragm. Anteromedially, the kidneys are covered by peritoneum; posteriorly, the 12th rib crosses the left kidney at a 45-degree angle, with approximately one-third or more of the left kidney superior to the inferior margin of the thoracic cage.[38–42] A fibrous envelope called the renal capsule covers the kidney and is firmly adherent to the renal substance. A potential space exists between the kidney and its capsule, which in abnormal situations (such as trauma and infection) may contain blood, pus, or urine.[38–42]

The renal sinus contains fat and fibrous tissue, renal vessels, nerves, and lymphatics. The sinus extends around the renal pelvis, the infundibula, and the calyces and is continuous with the perinephric fat. The renal arteries arise from the aorta and enter the renal hila. The renal veins lie anterior to the renal arteries, whereas the left renal vein usually runs between the aorta and the superior mesenteric artery.[38–42] The adrenal glands lie anterior and medial to the upper poles of kidneys and are bilobed V- or Y-shaped structures.

The anterior pararenal space contains the second and third parts of the duodenum, the pancreas, and the ascending and descending portions of the colon. It is limited anteriorly by the parietal peritoneum, and posteriorly by the renal fascia. The posterior pararenal space contains only fat and is bounded posteriorly by the transversalis fascia. The parietal peritoneum and transversalis fascia fuse laterally to form the lateroconal fascia. The anterior and posterior pararenal spaces communicate to a limited extent above and below the level of the renal vessels. Fascial planes are demonstrated as linear structures of soft tissue attenuation surrounded by low attenuation fat.[38–42] These fascial planes may unfuse and form a potential space between the perirenal and pararenal spaces to be filled with fluid; in particular, a sequelae of pancreatitis.

On unenhanced CT scans, the kidneys appear as oval structures with soft tissue (gray) attenuation surrounded by low attenuation (dark) perirenal fat (Fig. 11.3). They intensely (brightly) enhance with intravenous contrast. The appearance of the kidneys on MRIs depends on a number of factors, including the type of MR sequences, hydration, and contrast enhancement (Fig. 11.4). On T1-weighted images, the kidney presents with intermediate (gray) signal intensities similar to visceral organs and muscle. On T2-weighted images, the

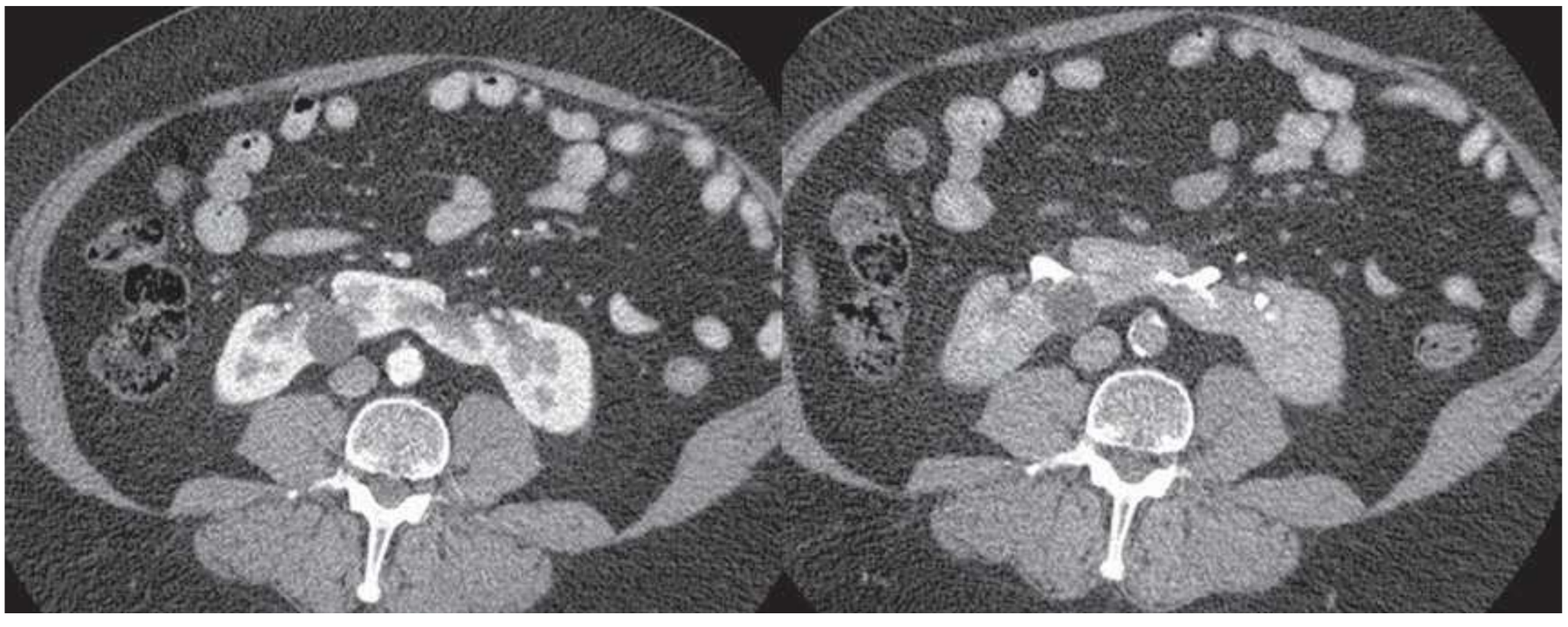

FIGURE 11.5 CT images of horseshoe kidney obtained at cortcomedullary (*left*) and delayed excretory phase (*right*). A small cyst is noted in the right kidney.

kidney is slightly hyperintense showing signal intensities similar to the spleen. The renal medulla is slighter darker on T1 images but is brighter on T2 images than the renal cortex. This is likely because of a greater unbound water (urine) content in the medulla.[25] Gadolinium contrast agents administered intravenously shorten T1 and enhance the renal parenchyma in T1-weighted images.[36,43–45] When lesion contrast enhancement is difficult to detect, a subtraction technique between unenhanced and enhanced T1-weighted images is required.

The calyces, renal pelvises, and ureters containing abundant water (urine) have low signals on T1-weighted images and high signals on T2-weighted images. The intraluminal signal intensities of the renal vessels vary widely depending on the MR sequences, imaging planes, and gadolinium contrast. The perirenal fat is bright on both T1- and T2-weighted images. The fat saturation technique suppresses the hyperintense perirenal fat signal and helps detect and characterize a renal lesion with fat, such as angiomyolipoma.

RENAL PATHOLOGIES

Congenital Variants of Renal Anatomy

Congenital and developmental variants of the kidney such as ectopic kidneys, horseshoe kidneys (Fig. 11.5), duplicated collecting systems, and various hypoplasia or dysplasia (Fig. 11.6) are routinely detected on cross-sectional imaging. An MRI is

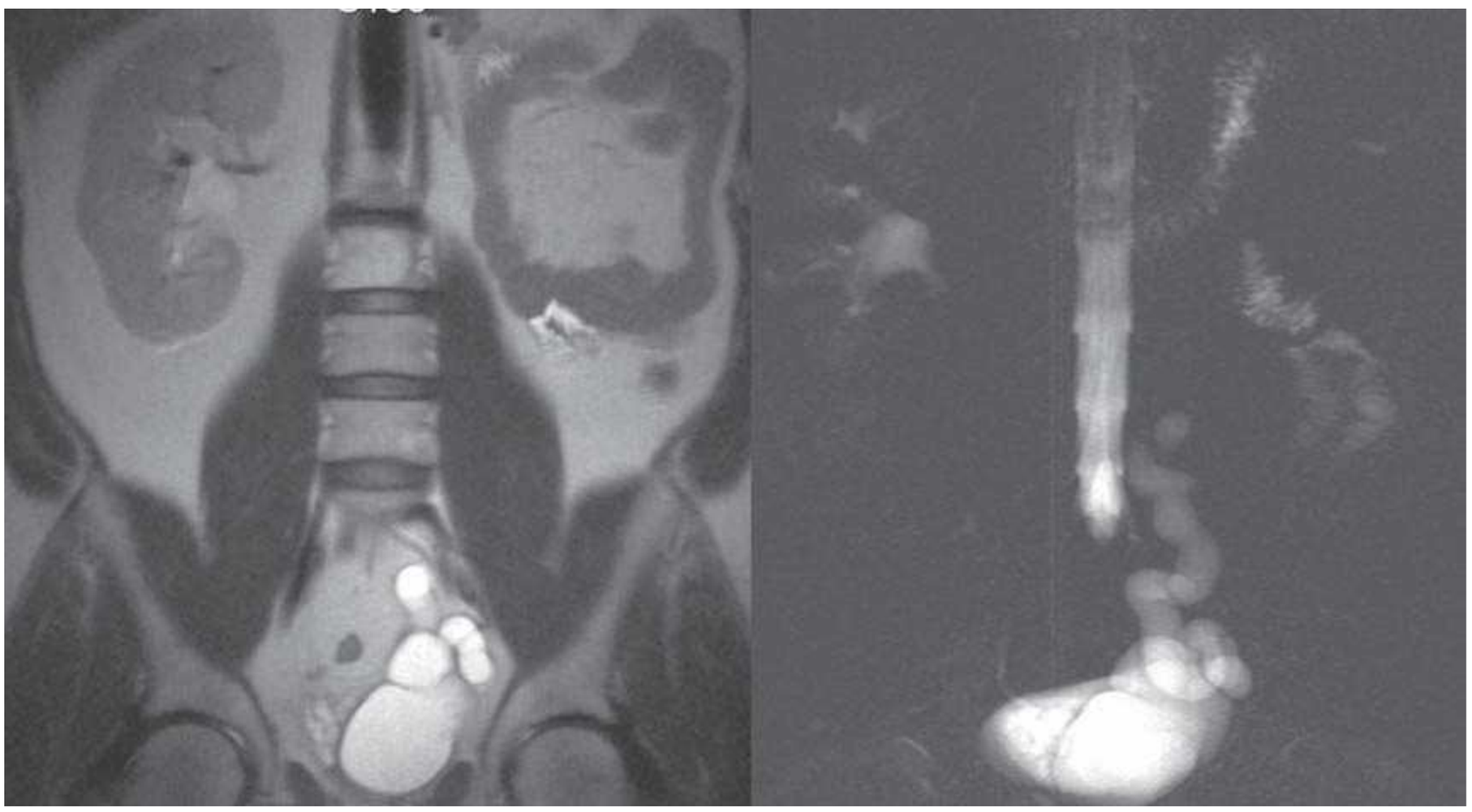

FIGURE 11.6 Left renal agenesis with dilated, tortuous ureteral remnant shown on T2-weighted MR (*left*) and MR urography (*right*). The right kidney shows compensatory hypertrophy.

FIGURE 11.7 CT images of kidneys obtained without intravenous contrast (*left upper*), at nephrographic phase with contrast (*right upper*), and at delayed excretory phase (*left lower*). Mild hydronephrosis in the left kidney caused by a distal ureteral calculus (*right lower*) is conspicuously demonstrated by excreted contrast filling the dilated collecting system.

particularly attractive as an imaging modality for the serial follow-up of pediatric patients with suspected renal anomalies because it requires no ionizing radiation and offers superb intrinsic contrast without exogenous contrast agents.[46,47]

Obstructive Disease

Unenhanced renal CT scans have emerged as an attractive alternative to intravenous urography (IVU) and ultrasound (US) imaging in patients with suspected renal colic. A CT scan allows us to evaluate the abdomen and the retroperitoneum for other disorders that mimic renal colic, including diverticulitis, appendicitis, an aortic aneurysm, and retroperitoneal fibrosis. The dilated, fluid-filled collecting system and ureter, along with the anatomic site, degree, and cause of obstruction can be evaluated on unenhanced images (Fig. 11.7). The acutely obstructed kidney may be enlarged and edematous. The renal execretion of contrast can be assessed on contrast-enhanced CT scans. With an acute obstruction, the usual transient, early cortical–medullary phase contrast enhancement is prolonged (persistent nephrogram) with a delayed excretion of contrast into the collecting system (Fig. 11.8).[3,6,27,28,36,43,48–56] Chronic obstruction may cause a marked distention of the fluid-filled collection system and an atrophy of the renal parenchyma.[3,6,27,28,36,43,48–56]

FIGURE 11.8 CT showing acute obstruction at the left uretero-pelvic junction with persistent cortico-medullary enhancement (compare the pattern of enhancement to the right kidney).

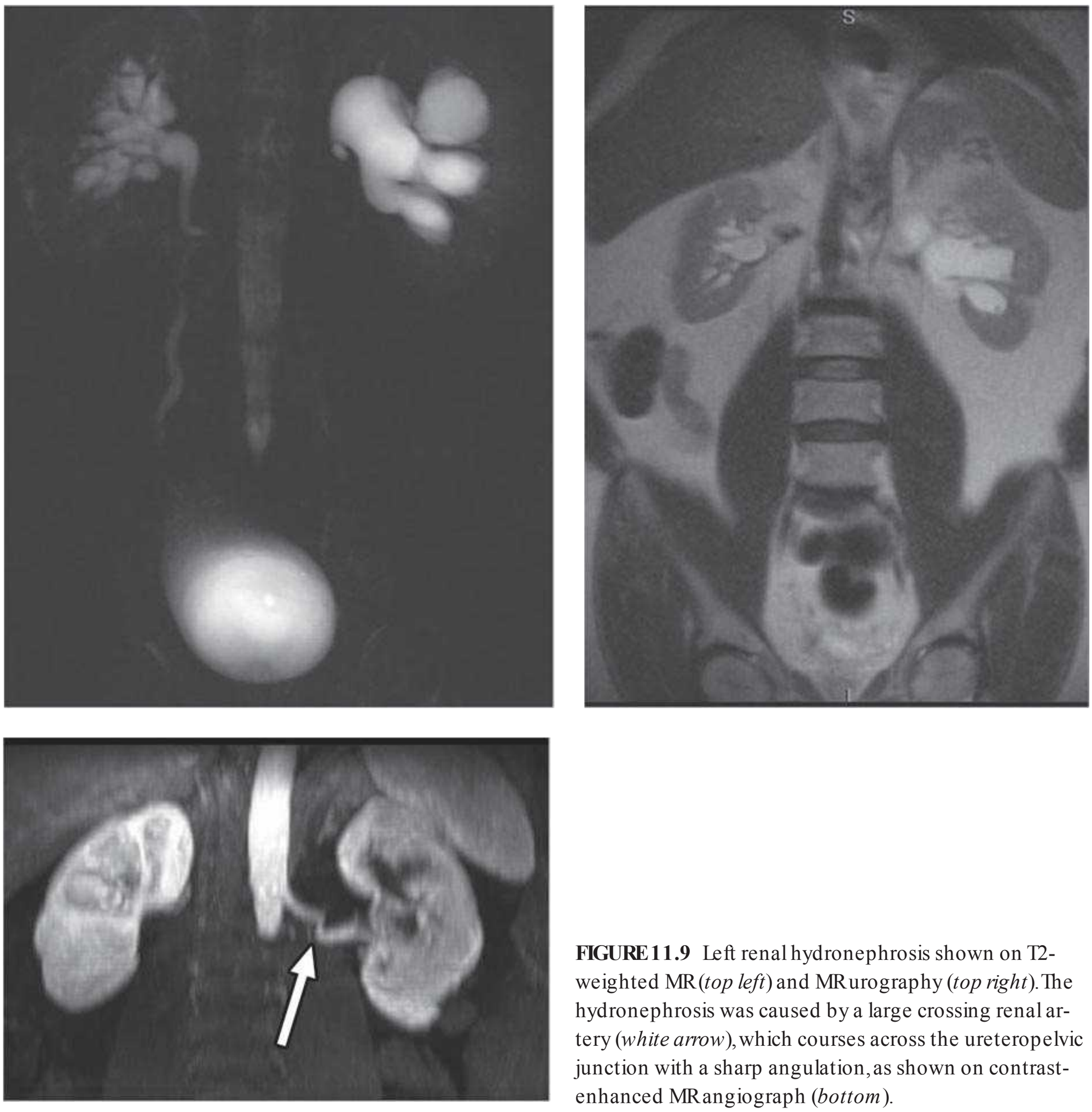

FIGURE 11.9 Left renal hydronephrosis shown on T2-weighted MR (*top left*) and MR urography (*top right*). The hydronephrosis was caused by a large crossing renal artery (*white arrow*), which courses across the ureteropelvic junction with a sharp angulation, as shown on contrast-enhanced MR angiograph (*bottom*).

Although an MRI is not commonly used as the first-line diagnostic imaging modality for the evaluation of suspected obstructive disease, the ureteral, pelvic, and calyceal dilatation caused by a distal obstruction can be readily delineated on transaxial, sagittal, or coronal MRIs. Gadolinium contrast is not necessary to determine the presence of an obstruction. In particular, an MRI that uses heavily T2-weighted images without gadolinium contrast has been shown to be accurate in detecting an obstruction (Fig. 11.9).[3,6,27,28,36,43,48–56]

Nephrolithiasis

Because CT scans provide an accurate, rapid, and safe evaluation of suspected renal calculi without contrast, it has replaced IVU for this application. Unenhanced CT scans have been reported to have sensitivities ranging from 96% to 100% and specificities ranging from 92% to 100% for the diagnosis of nephrolithiasis or urolithiasis.[57–63]

Regardless of the chemical composition, renal and ureteral calculi are generally radiodense on CT scans (with the rare exception of indinavir-induced stones). Thus, cystine and urate calculi that are difficult to detect on conventional abdominal radiographs can be readily diagnosed on unenhanced CT scans. Crixivan (indinavir sulfate), a protease inhibitor used to treat patients with HIV, can precipitate in the urinary system forming radiolucent stones that may not be directly visualized on CT scans. When nephrolithiasis is suspected, the initial CT scan should be obtained before the administration of contrast agents because the high-attenuation contrast excreted into the collecting system may obscure underlying calculi.

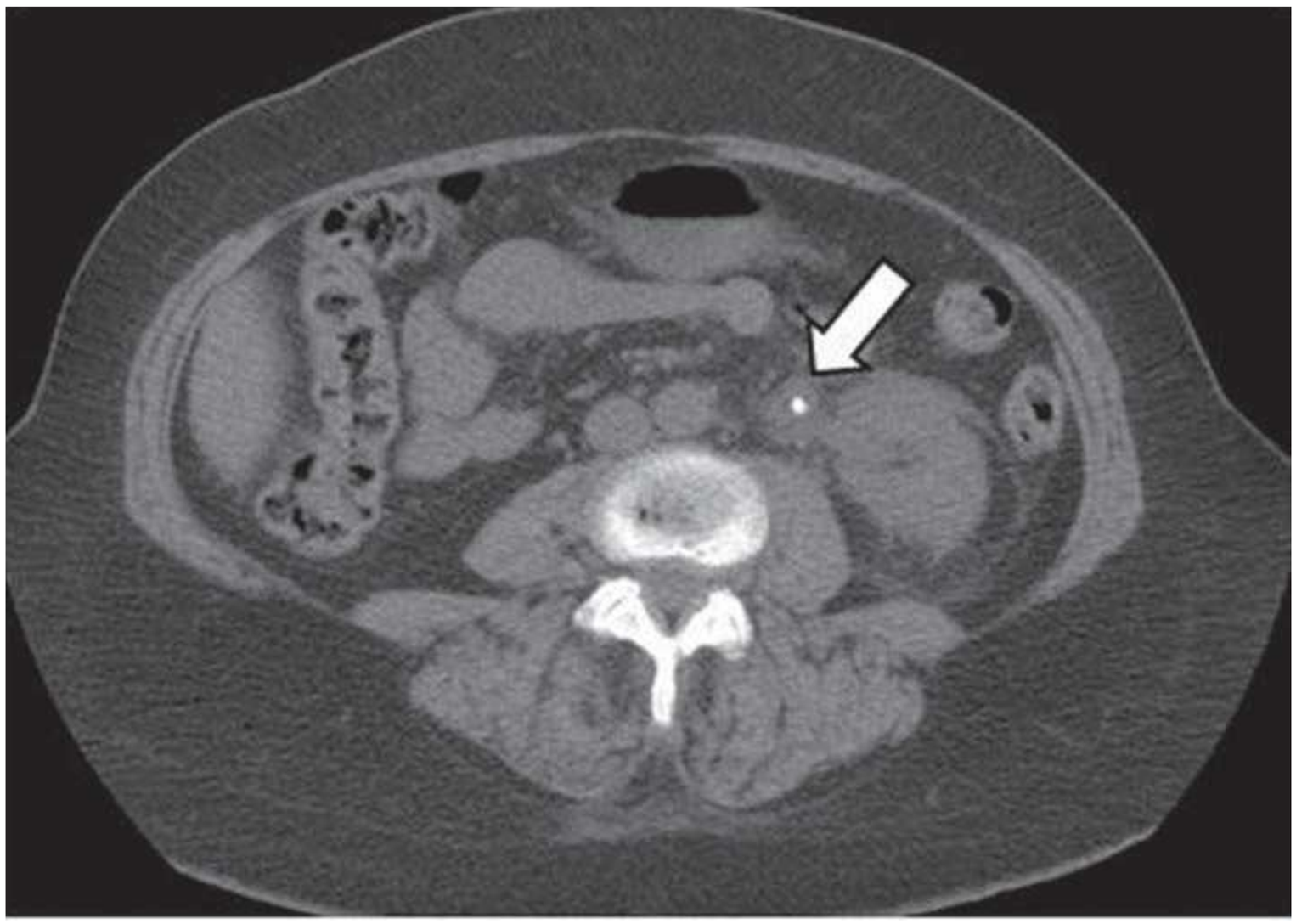

FIGURE 11.10 Unenhanced CT showing a hyperattenuating calculus at the left uretero-pelvic junction with peri-nephric and peri-ureteric soft tissue stranding consistent with acute left renal colic due to nephrolithiasis.

The most common locations for an obstruction by a stone are the natural anatomic points of narrowing: the ureteropelvic junction (Fig. 11.10), the pelvic brim where the ureter crosses the iliac vessels, and the ureterovesical junction. The most obvious sign of a ureteral stone on a CT scan is a focus of high attenuation (similar to bone) within the ureter.[57–63] Secondary signs of an obstruction include ureteral dilatation, asymmetric inflammatory change of the perinephric fat, hydronephrosis, and nephromegaly. An obstructing stone at the ureterovesical junction may be difficult to differentiate from a stone that recently passed into the bladder. In such a case, scan the patient in a prone position and the stone that falls to the anterior portion of the bladder is a stone that has passed.[57–63]

Renal or ureteral calculi are not directly visible on an MRI because they do not produce MR signals. They may be indirectly identified as foci of a signal void within the renal parenchyma, the collecting system, or ureters (Fig. 11.11). However, other objects including air, metal, and sutures also present as sites of signal void on an MRI.

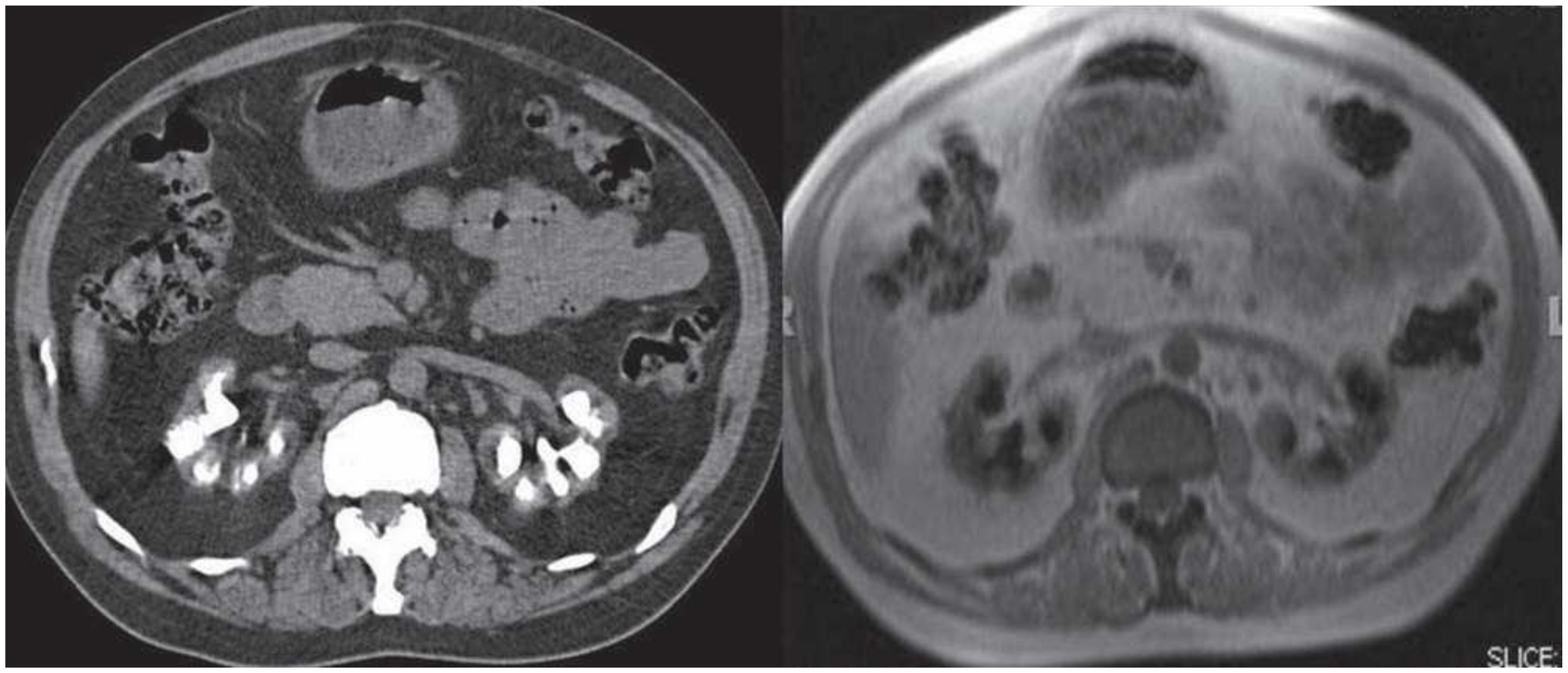

FIGURE 11.11 Extensive medullary calcinosis is shown as multiple hyperattenuating foci in the bilateral kidneys on unenhanced CT (*left*) but only as signal voids on T1-weighted MRI (*right*), undifferentiated from gas in the gastrointestinal tract.

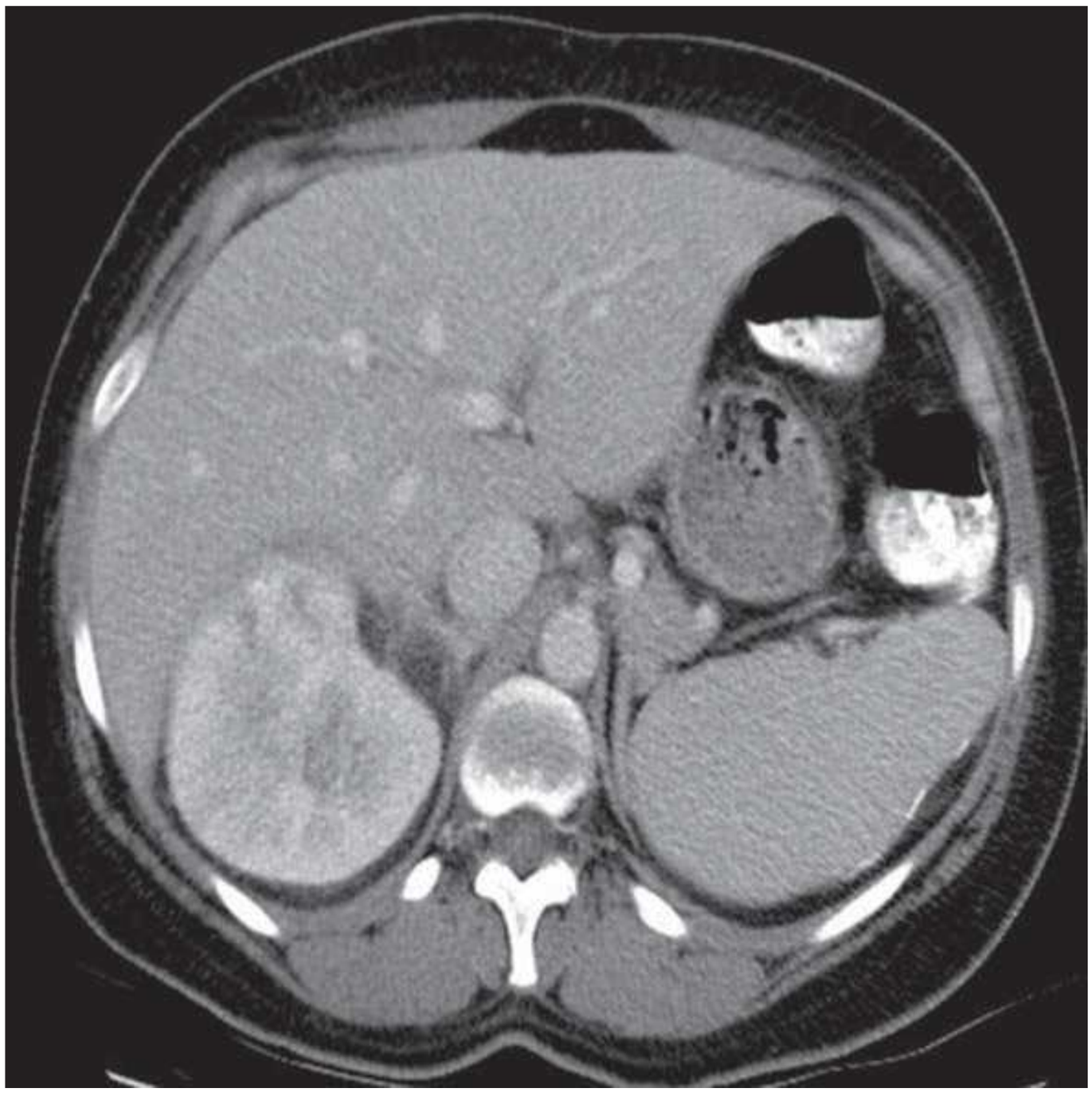

FIGURE 11.12 Contrast-enhanced CT in a patient with clinical symptoms of acute pyelonephritis showing striated nephrogram in an edematous right kidney with multiple linear non-enhancing areas.

Inflammatory Disease

Acute Pyelonephritis

Acutely inflamed kidneys may present with a range of findings on a CT scan. These include renal enlargement, heterogeneous patterns of contrast enhancement or striated nephrograms (Fig. 11.12), and pelvicaliceal air. Perirenal effusions and a thickening of the perirenal fascia may be seen with severe inflammation. A CT scan is also useful in depicting long-term sequelae of renal infections, renal parenchymal scarring and atrophy, and deformities of the collecting system (Fig. 11.13).[30,40,64–66] A CT scan is also superior to ultrasonography in detecting and delineating renal and perirenal abnormalities that are associated with pyelonephritis and abscesses.

Acute pyelonephritic kidneys may show loss of corticomedullary distinction on T1-weighted MRIs. Perirenal edemas may produce a decrease in the signal intensity of the surrounding fat and the thickening of renal fascia. Areas of inflammation and abscess cavity walls demonstrate contrast

Figure 11.13 Left kidney with recurrent acute pyelonephritis (*left*) resulting in atrophy shown in follow-up CT (*right*).

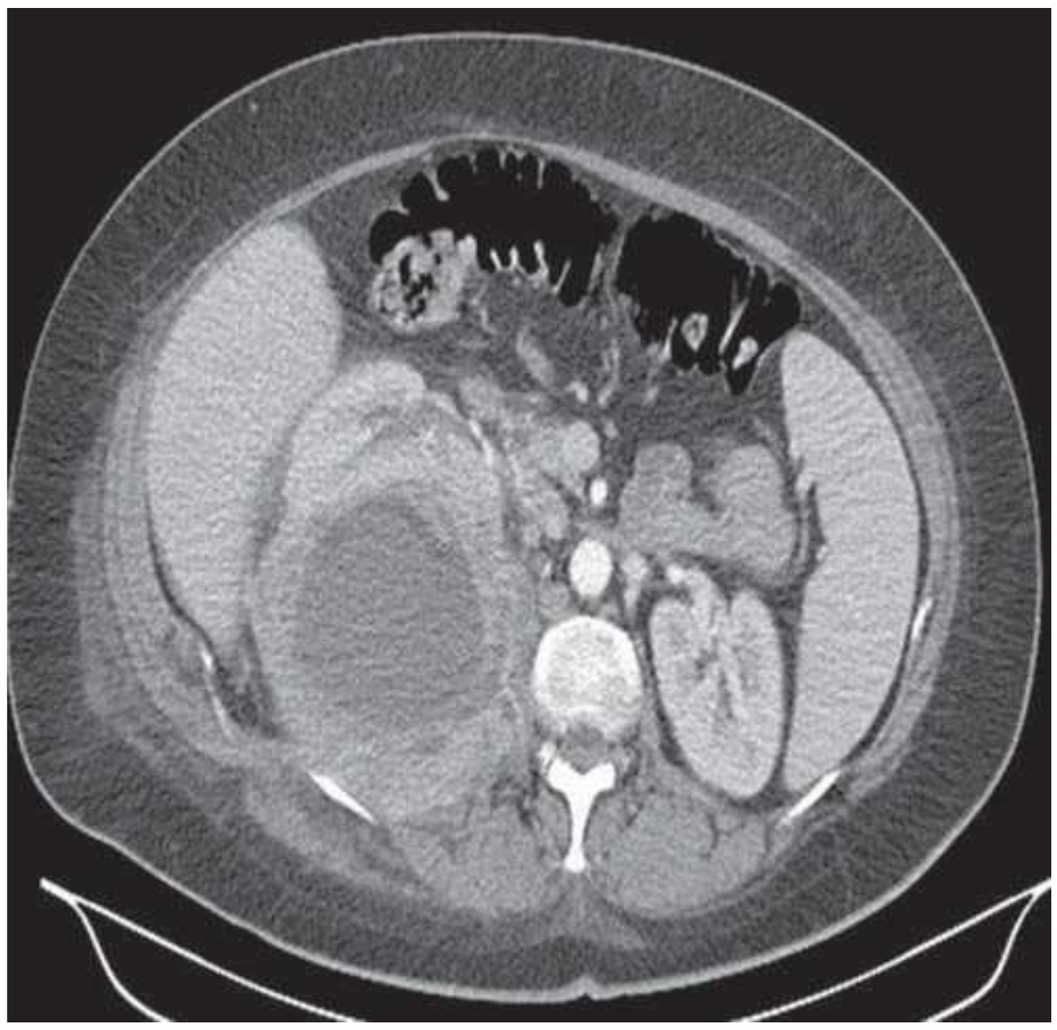

FIGURE 11.14 Contrast-enhanced CT showing a large, thick-walled abscess arising from the posterior cortex of the right kidney and extending into the adjacent posterior pararenal space.

enhancement after the administration of gadolinium contrast agents. On the T2-weighted images with fat saturation, edema and an inflammatory reaction may present with areas of an increased signal in the renal parenchyma and perirenal space.[30,41,66]

Renal Abscesses

Renal abscesses appear as well-defined collections of fluid in nonlobar distributions. An abscess may present with a thick wall that enhances after the administration of contrast agents in CT scans or MRIs and may contain air (Fig. 11.14). Abscesses may extend or rupture into the perirenal fat. A CT scan is superior to sonography in delineating abscesses and the pararenal extent of inflammation and is preferred when intervention is planned.[67,68] Abscesses may show varied signal intensity on MRIs depending on the content of fluid within the abscesses.

Fungal Infections

Fungal infections of the kidney are rare and are seen in immunocompromised patients. CT findings include a focal or global lack of contrast excretion, renal mass, renal enlargement, and filling defects of soft-tissue masses within the renal collecting system.[68]

Xanthogranulomatous Pyelonephritis

Xanthogranulomatous pyelonephritis is an uncommon inflammatory condition that often follows chronic renal obstruction. It produces intrapelvic and intracalyceal collections of fluid or fatty material. The renal parenchyma is often atrophic and is replaced by accumulated fat, pus, and cellular debris and calcification.[69] Calcification in the collecting system and perirenal abscesses are frequently present.

Cystic Disease

Cysts in the kidneys are extremely common and an uncomplicated renal cyst can be diagnosed reliably by a CT scan or an MRI. Simple renal cysts are variable in size and number. On a CT scan, a simple cyst usually appears as a well-defined rounded mass of water attenuation (0 to 20 HU), with an imperceptible wall and no enhancement after the administration of contrast agents. The MRI appearance of a simple renal cyst is characterized by a sharply demarcated, homogeneous, and hypointense mass on T1-weighted images. The simple cyst becomes uniformly hyperintense on T2-weighted images and shows no enhancement following contrast medium administration.[70–73] Complex renal cysts may be irregular in shape and have thicker or calcified walls. Fluid within complex cysts may present with high attenuation (hyperdense cysts) on a CT scan or complex signal intensity on an MRI (bright T1 and dark T2 or bright T1 and T2 images); in fact, they may simulate solid tumors. Such lesions require a further diagnostic evaluation with a dedicated renal CT scan or an MRI protocol, including scanning before and after the administration of a contrast agent. The degree of contrast enhancement within a lesion is critical in the characterization of the renal lesion.

Cystic renal lesions are often characterized according to the Bosniak classification system.[71,72] Class I cysts are simple benign cysts. Class II cysts have one or more thin (<1 mm) septa running through them, thin areas of mural calcification, or fluid contents of increased attenuation; they do not enhance after the administration of contrast medium and are benign (Fig. 11.15). Class III cysts are more complicated and contain thickened septa, nodular areas of calcification, or solid nonenhancing areas. Such lesions are suggestive of malignancy and should be biopsied or surgically explored, although fewer than half will turn out to be malignant. Class IV cystic masses are clearly malignant, with solid enhancing nodules or irregular walls, and should be treated accordingly (Fig. 11.16). A subcategory, IIF, has been suggested for lesions with multiple class II features, and these require follow-up.[65,70,74–81]

Parapelvic Cysts

Extraparenchymal cysts commonly occur in the renal sinus (parapelvic or peripelvic cysts). These cysts are often discovered incidentally, are frequently multiloculated, and may be large enough to displace hilar fat and compress adjacent renal parenchymas.[65,70,74–81] Although they do not communicate with the collecting system, they may simulate hydronephrosis because of their proximity to

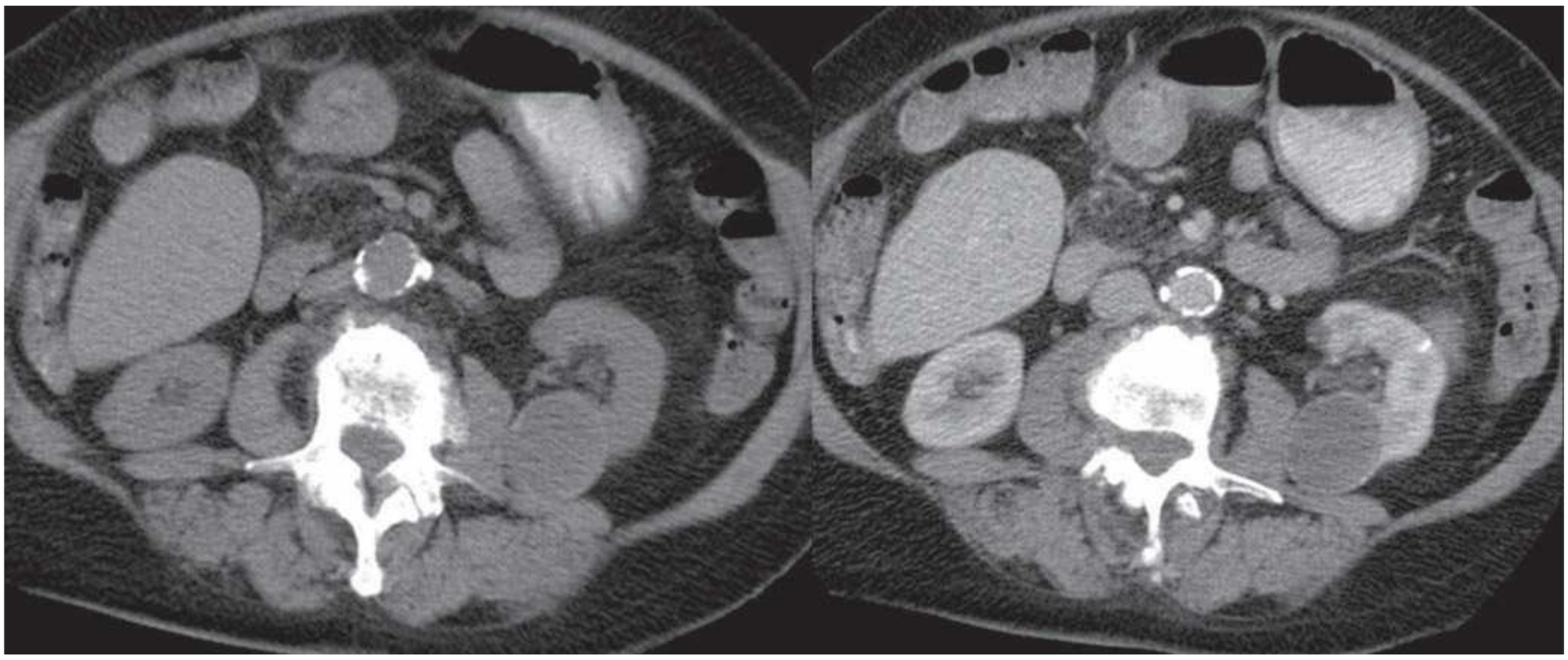

FIGURE 11.15 Bosniak class II cyst in the left kidney with slightly higher attenuation contents and subtle peripheral hyperdense rim on the pre-contrast CT but no contrast enhancement on the post-contrast CT.

the collecting system. When the diagnosis is uncertain, a delayed CT scan or an MRI after the administration of contrast agents can help differentiate unenhanced parapelvic cysts from a contrast-enhanced dilated collecting system (Fig. 11.17).

Autosomal Dominant Polycystic Kidney Disease

In individuals with a positive family history, the diagnosis of autosomal dominant polycystic kidney disease (ADPKD) can be established by radiologic imaging. The reported sonographic criteria[82] cannot be used with a CT scan or MRI because these imaging modalities have a higher sensitivity than US for the detection of renal cysts, particularly small cysts.[83,84] The kidneys are affected bilaterally in almost all instances, but may be quite asymmetric. Early in the disease, the kidney is close to normal in size with a substantial amount of normal renal parenchyma. However, with disease progression, the kidneys gradually enlarge as the cysts increase in number and size and replace normal parenchymas (Fig. 11.18).[85]

Most ADPKD renal cysts are simple cysts but increase with complex cysts as the disease progresses. The CT attenuation and MRI signal intensity of complex cysts affected by hemorrhage or infection may vary. ADPKD patients with

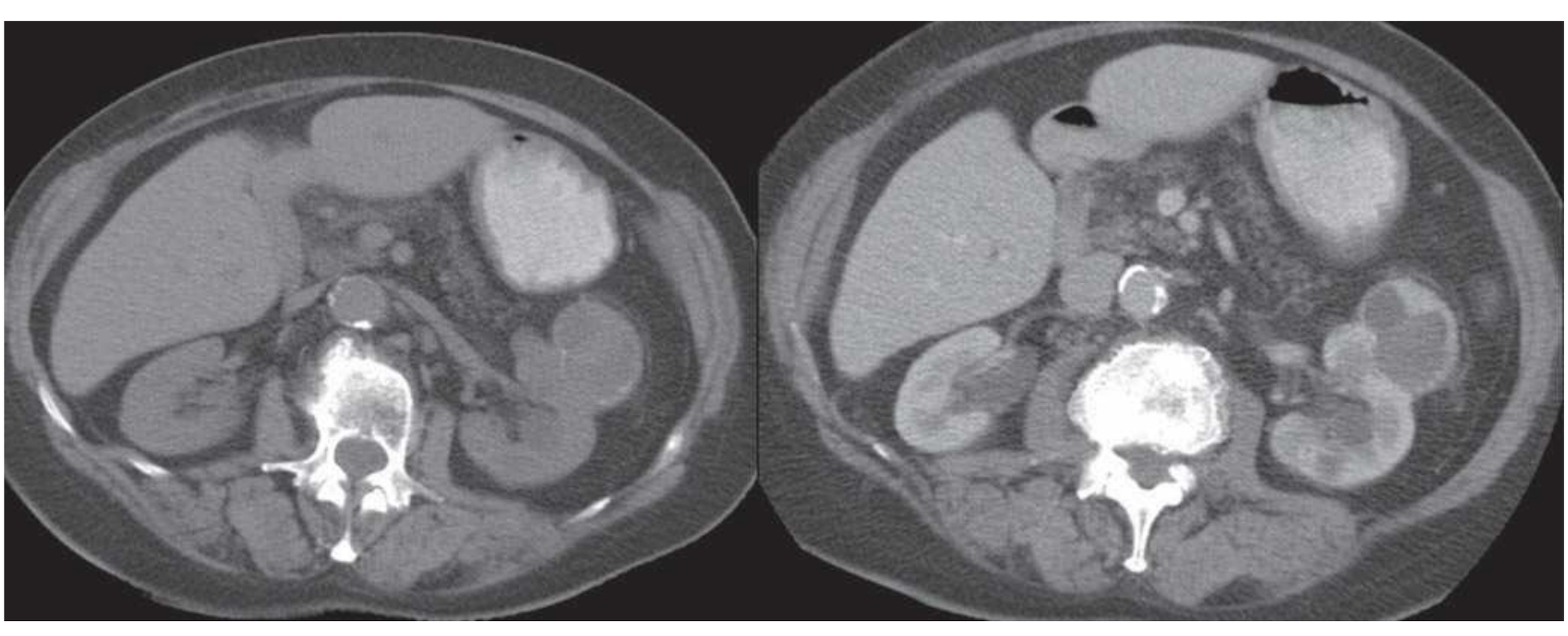

FIGURE 11.16 Pre- and post-contrast CT of Bosniak class IV cyst in the left kidney demonstrating peripheral nodular enhancement.

FIGURE 11.17 Bilateral parapelvic cysts are shown as bright structures on axial T2 MRI (*left*) and water-attenuation cystic structures on contrast-enhanced axial CT (*middle*) and coronal CT (*right*). The parapelvic cysts on axial CT do not enhance but are surrounded by delayed excretion of contrast medium within the collecting system. An incidental large abdominal aortic aneurysm is noted.

clinically suspected renal infection or pain are referred for a CT scan or an MRI evaluation of intracystic infection or hemorrhage.[65,70,74–81,85,86] But this is often difficult because the attenuation and signal intensity values of these cysts vary depending on the presence of blood products, proteinaceous mucoid material, or simple cyst fluid. Sequential studies allow for the evaluation of a fresh hemorrhage and the resolution of hematomas.

Acquired Cystic Disease Associated with Chronic Dialysis

Patients with acquired cystic disease associated with hemodialysis typically present with multiple bilateral cysts of varying size in small kidneys (Fig. 11.19). Although sonography is usually used for a diagnostic evaluation, small fibrotic end-stage kidneys may be difficult to image with sonography.[87] A contrast-enhanced CT scan or MRI is more sensitive

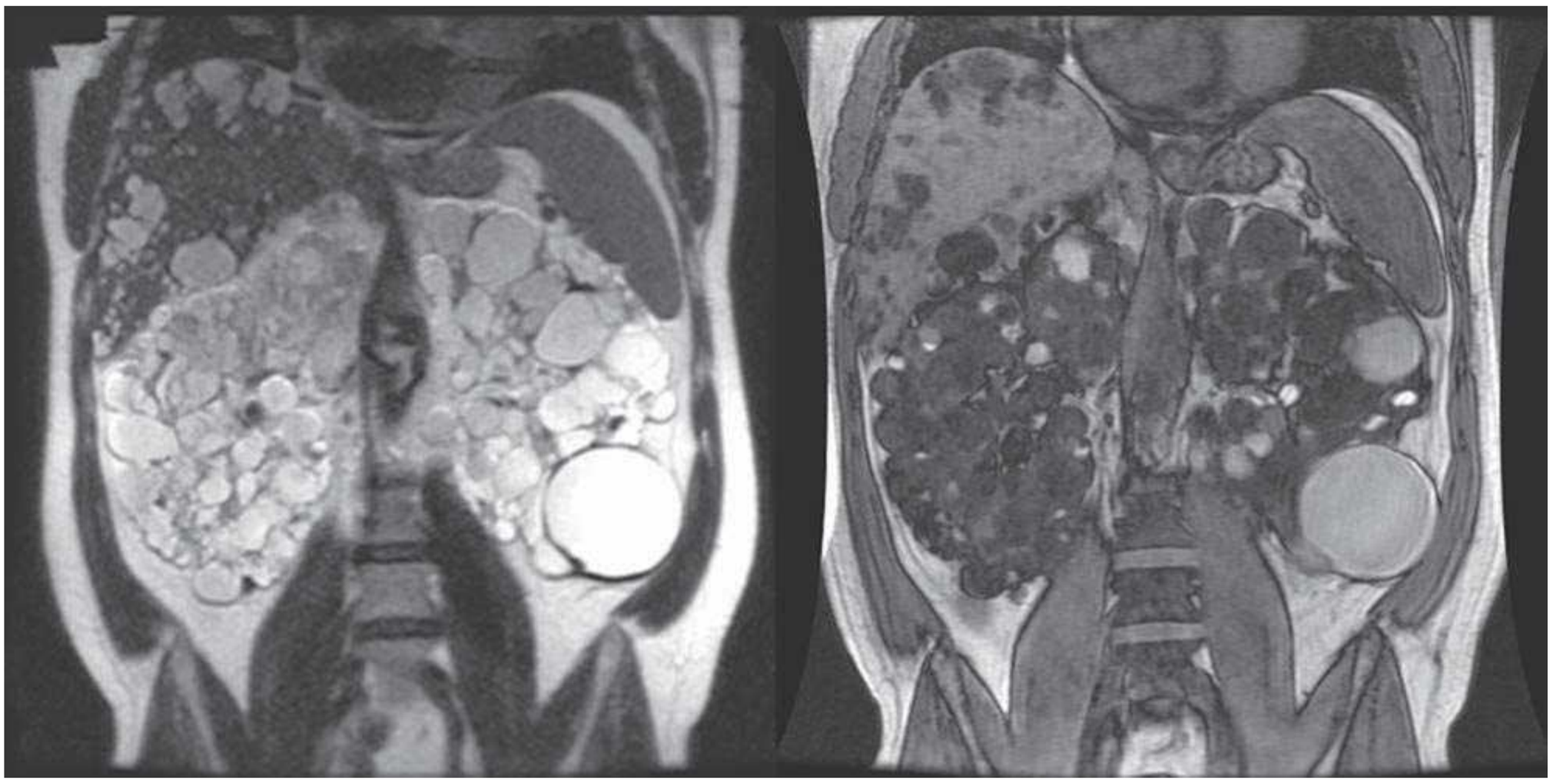

FIGURE 11.18 ADPKD on coronal MR images. Innumerable cysts occupying markedly enlarged bilateral kidneys on T2 (*left*) and T1 (*right*) MR images. Simple cysts are of bright T2 and dark T1 signal intensity, whereas complex cysts present with intermediate to bright T1 signal intensities. Extensive hepatic cysts are also present.

FIGURE 11.19 Contrast-enhanced CT showing multiple cysts of varying sizes in both kidneys that are markedly atrophied.

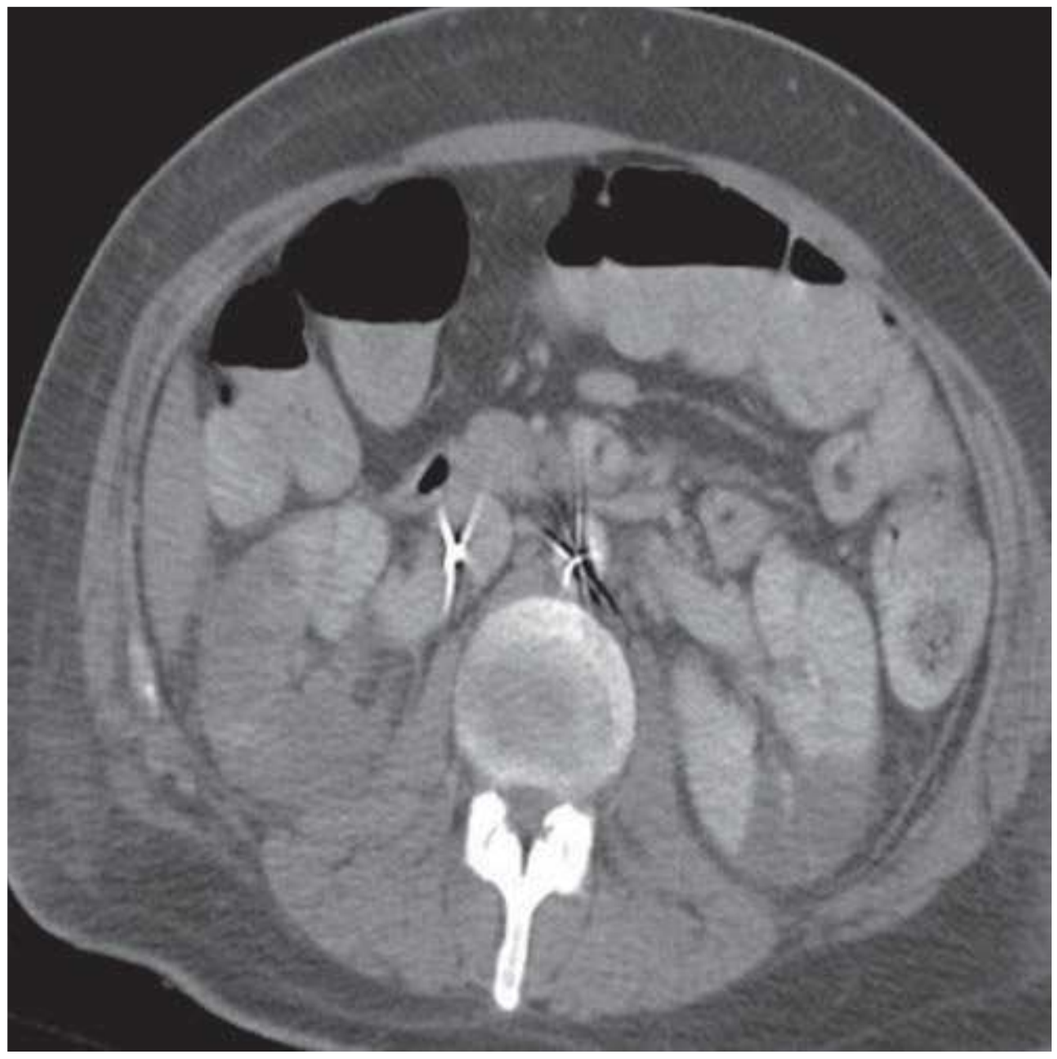

FIGURE 11.20 Contrast-enhanced CT demonstrating bilateral multiple renal infarcts as wedge-shaped nonenhancing low-attenuation areas.

to determine the extent of the disease, cyst complications, and renal carcinomas.[88–90] Because of limited or an absent renal function of these individuals and the presence of numerous simple and complex cysts, an MRI is the preferred modality for the evaluation of potential renal malignancies. Nevertheless, a contrast-enhanced CT scan may also be used if patients are receiving dialysis.[90]

Vascular Pathologies

Renal infarcts typically present as clearly marginated wedge-shaped peripheral areas of low attenuation on contrast-enhanced CT scan (Fig. 11.20) or low signal intensity on contrast-enhanced MRI. A parenchymal atrophy caused by chronic vascular insufficiency may be detected on a CT scan or MRI.

A CT scan or an MRA is used to assess the number and size of the renal arteries, which is crucial for the evaluation of a renal donor for transplant. A CTA and an MRA have largely replaced conventional catheter angiography for this application. A CTA and an MRA can also demonstrate renal artery aneurysms or stenosis (Fig. 11.21), arteriovenous malformations, and focal or diffuse stenoses caused by atherosclerosis, connective tissue disease, or fibromuscular dysplasia. Although the 3D gadolinium-enhanced protocol is the preferred technique for an MRA, new time of flight MR protocols have been introduced to image renal vessels without gadolinium for patients with a severely compromised renal function.

Renal vein thrombosis typically presents with intraluminal filling defects and vein enlargement (Fig. 11.22). Acute venous occlusion may result in renal enlargement and parenchymal edema and, occasionally, hemorrhagic infarction. A contrast-enhanced CT scan or an MRI may show a persistent nephrogram and delayed contrast excretion. A parenchymal atrophy and the development of venous collaterals may be followed with chronic renal vein thrombosis.[3,91–98]

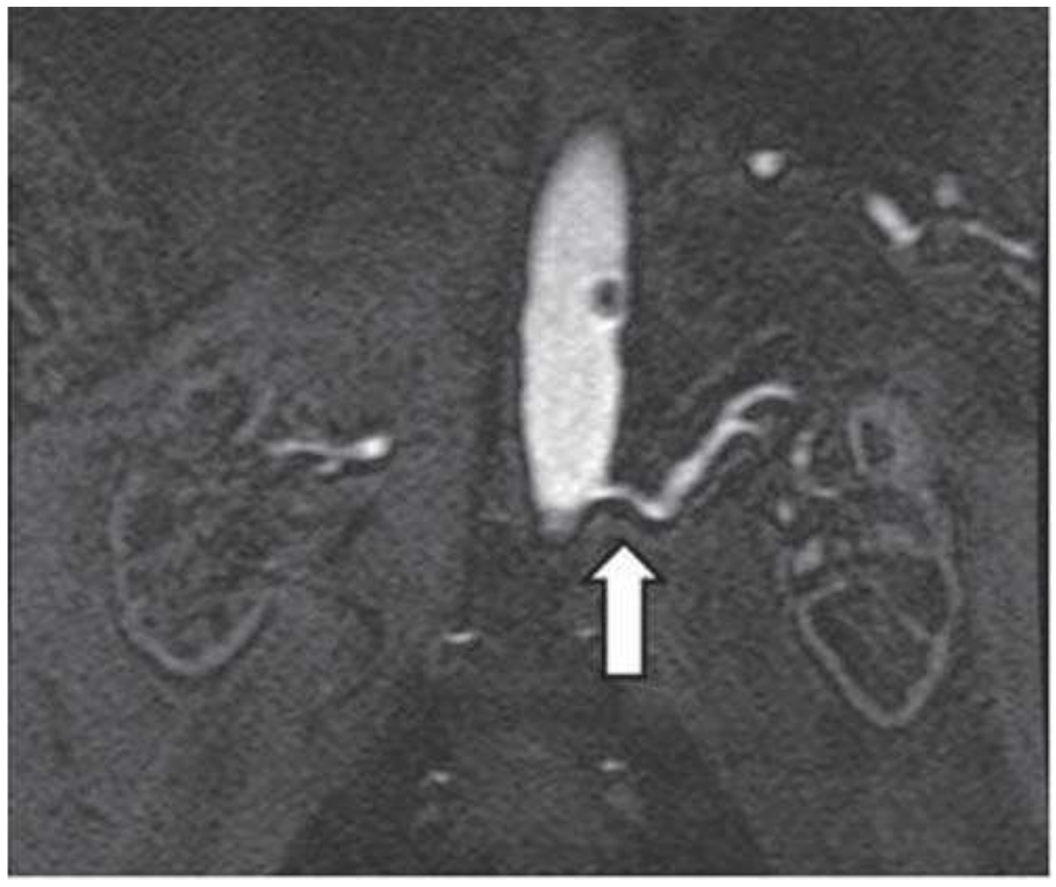

FIGURE 11.21 Contrast-enhanced coronal MR angiography showing a focal stenosis near the origin of left renal artery (*arrow*).

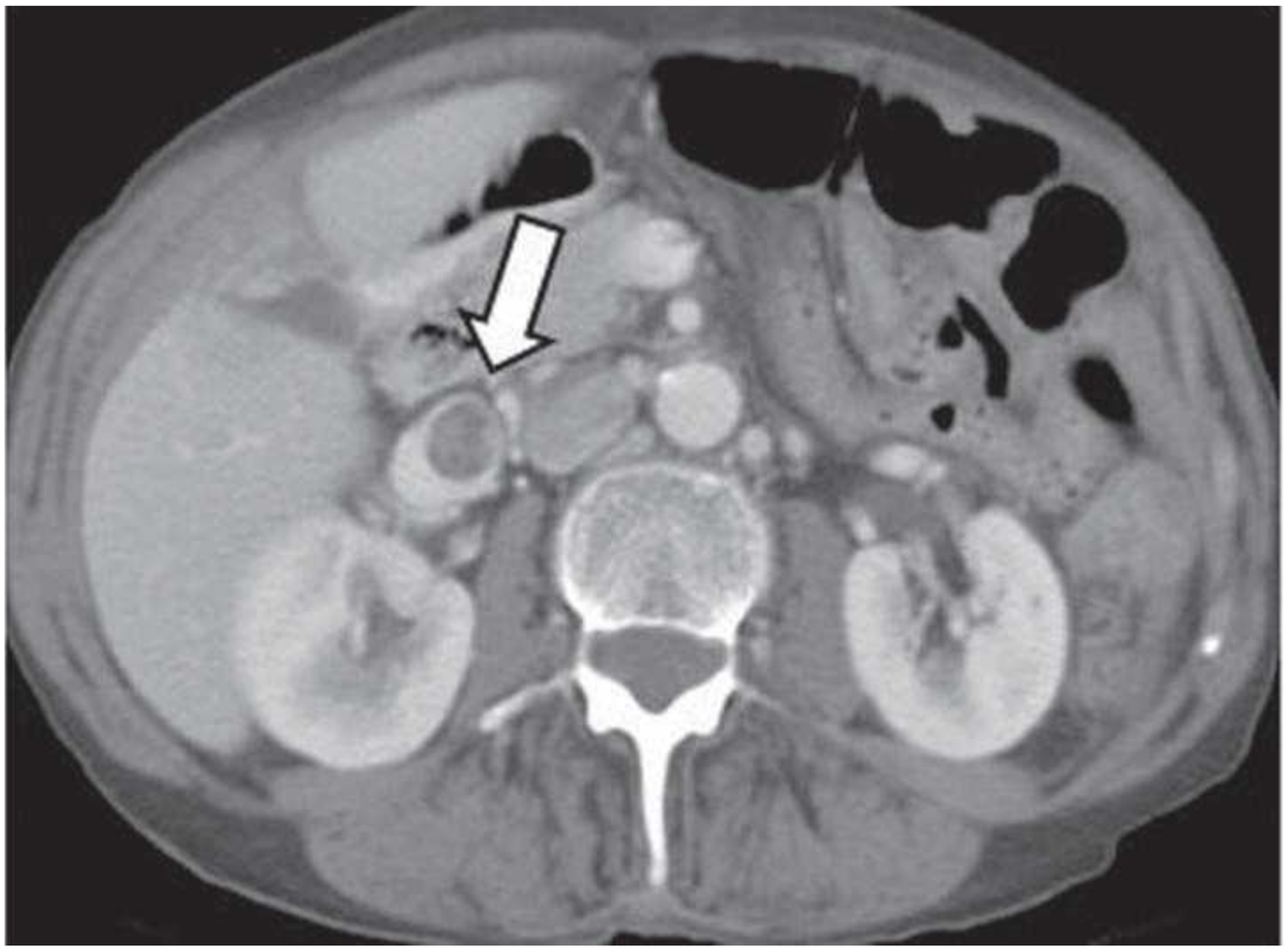

FIGURE 11.22 Contrast-enhanced CT showing a low-attenuation filling defect (*arrow*) in an expanded right renal vein consistent with renal vein thrombosis.

Renal Transplant Evaluation

The structural integrity of renal allografts and common peritransplant complications (hematomas, urinomas, lymphoceles, and abscesses) can be readily assessed with a CT scan or an MRI. However, the characterization of graft dysfunction, such as the differentiation of rejection and acute tubular necrosis (ATN), remains challenging by any radiologic imaging method. Recent applications of functional MRI techniques including diffusion, blood oxygen level dependent (BOLD), and sodium MRI are promising for the noninvasive evaluation of graft dysfunction[16] but are not ready for routine clinical application. A CTA or an MRA are very useful for the evaluation of the allograft vasculature including arterial or venous stenosis and aneurysm.[99,100]

Renal Tumors

The evaluation of hematuria is a common reason for a urology referral. Historically, the workup included IVU, urine cytology, and cystoscopy. Other imaging modalities available for hematuria workup include a CT scan, ultrasonography, an MRI, and a retrograde pyelography. In particular, MDCT is increasingly used as a single-imaging comprehensive evaluation of a patient with hematuria. The unenhanced phase of the CT scan is highly reliable for diagnosing urolithiasis. The enhanced nephrographic phase aids in the detection of renal parenchymal masses. The excretory phase with 3D reformation allows for the evaluation of the entire urothelium. MDCT has been shown to have high sensitivity in detecting upper tract urothelial cancers. Some investigators add a corticomedullary phase to characterize the renal artery and vascularity of parenchymal renal masses. One concern about this comprehensive CT technique is the radiation dose to the patient, and some investigators advocate not covering the entire abdomen and pelvis in all phases of the examination in order to limit the radiation dose.[32,37,52,56]

An MRI is equivalent to a CT scan in its ability to detect renal lesions of approximately 1 cm[56] and in detecting a lymphadenopathy.[56] An MRI detects polar lesions better than a CT scan and has up to 100% sensitivity in detecting a renal vein invasion. Most renal tumors, including benign lesions, enhance on CT scans and MRIs. T1-weighted chemical-shift MRIs are highly reliable for the detection of fat content within renal lesions. With fat saturation sequences, the fatty portions of a mass drop in signal, which is diagnostic of a fat-containing renal mass such as angiomyolipoma. After the exclusion of angiomyelolipomas and in the absence of lymphoma and metastatic disease, all other enhancing renal lesions represent surgical lesions. Unfortunately, neither CT scans nor MRIs can reliably differentiate some benign enhancing tumors such as oncocytomas from renal cell carcinomas.[32,37,56,65,71,94,101–109]

Benign Tumors

Angiomyolipoma

Angiomyolipomas are benign lesions composed of variable amounts of fat, smooth muscle, and abnormal blood vessels. They occur spontaneously in the general population, mainly in women in the fifth decade of life. In patients with tuberous sclerosis, they occur at a much younger age and are frequently multiple, with an incidence of 50% to 80%.[110,111] A confident diagnosis can be made with a CT scan if the fatty tissue predominates. The tumor may grow very large in size and may extend into the perinephric space. An intralesional hemorrhage often occurs. The MRI appearance of angiomyolipomas depends on the amount of fat, smooth muscle, and vessels within the lesion.

FIGURE 11.23 Angiomyolipoma (*arrow*) in the left kidney with bright signal intensity similar to the surrounding body fat on T1-weighted MRI without fat saturation (*left*) but showing a signal drop on T1-weighted with fat saturation (*right*).

Angiomyolipomas composed predominantly of fat present with signal intensity on T1- and T2-weighted images similar to the surrounding fatty structures and demonstrate a signal drop on the fat suppression sequences (Fig. 11.23).[65,102,110,112]

Renal Oncocytomas

Renal oncocytomas are rare tumors that typically appear as smoothly marginated, homogeneously enhancing solid masses. These masses may demonstrate a characteristic central linear area of lower attenuation (stellate central scar) on a contrast-enhanced CT scan. But, this appearance on CT is found in only a small proportion of these tumors and is not specific, and the diagnosis of these benign masses necessitates an operative biopsy/resection (Fig. 11.24).[7,65,76,105,107] A recent CT study reported that the segmental enhancement inversion between two phases of a contrast-enhanced CT scan was significantly more frequent in oncocytomas than in renal cell carcinomas and could be diagnostically useful in differentiating the two.[113]

Renal Adenomas

Renal adenomas are indistinguishable from other solid renal masses on CT scans or MRIs. They may show variable contrast enhancement and may present as a contour abnormality or distortion of intrarenal anatomy, necessitating further workup and intervention.[114]

Malignant Tumors

Renal Cell Carcinoma

Renal cell carcinomas are a relatively common malignancy. Their appearance on CT scans and MRIs varies with the size and tumor vascularity. Tumors may distort the renal contours or alter intrarenal architecture (Fig. 11.25). On a CT scan, their attenuations are similar to those of the surrounding renal parenchyma in unenhanced images. Tumors often enhance heterogeneously on enhanced CT scans, with central areas of low attenuation (Fig. 11.26). On an MRI, tumors demonstrate a variable signal on both T1- and T2-weighted images. The most common appearance is a heterogeneous mass of low-to-intermediate signal on T1-weighted images that increases in signal intensity on T2-weighted images. Dynamic CT scans or MR scanning after a bolus of contrast may demonstrate an intense enhancement of relatively vascular tumors and retroperitoneal feeding of collateral vessels.[93,115–117] An extension of the tumor into the perirenal

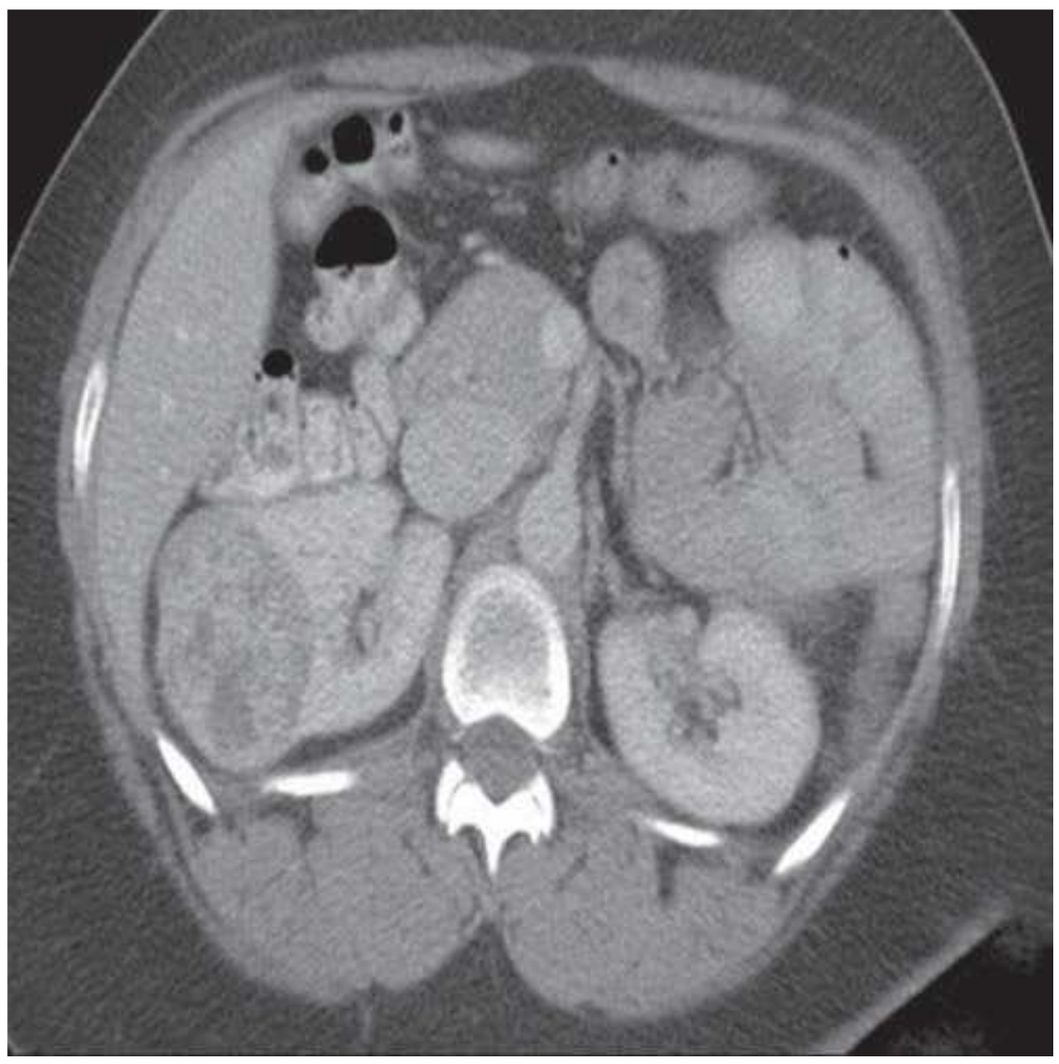

FIGURE 11.24 Contrast-enhanced CT showing an oncocytoma in the right kidney with mixed areas of enhancement and low attenuation. This is difficult to differentiate from renal cell cancer based on imaging alone.

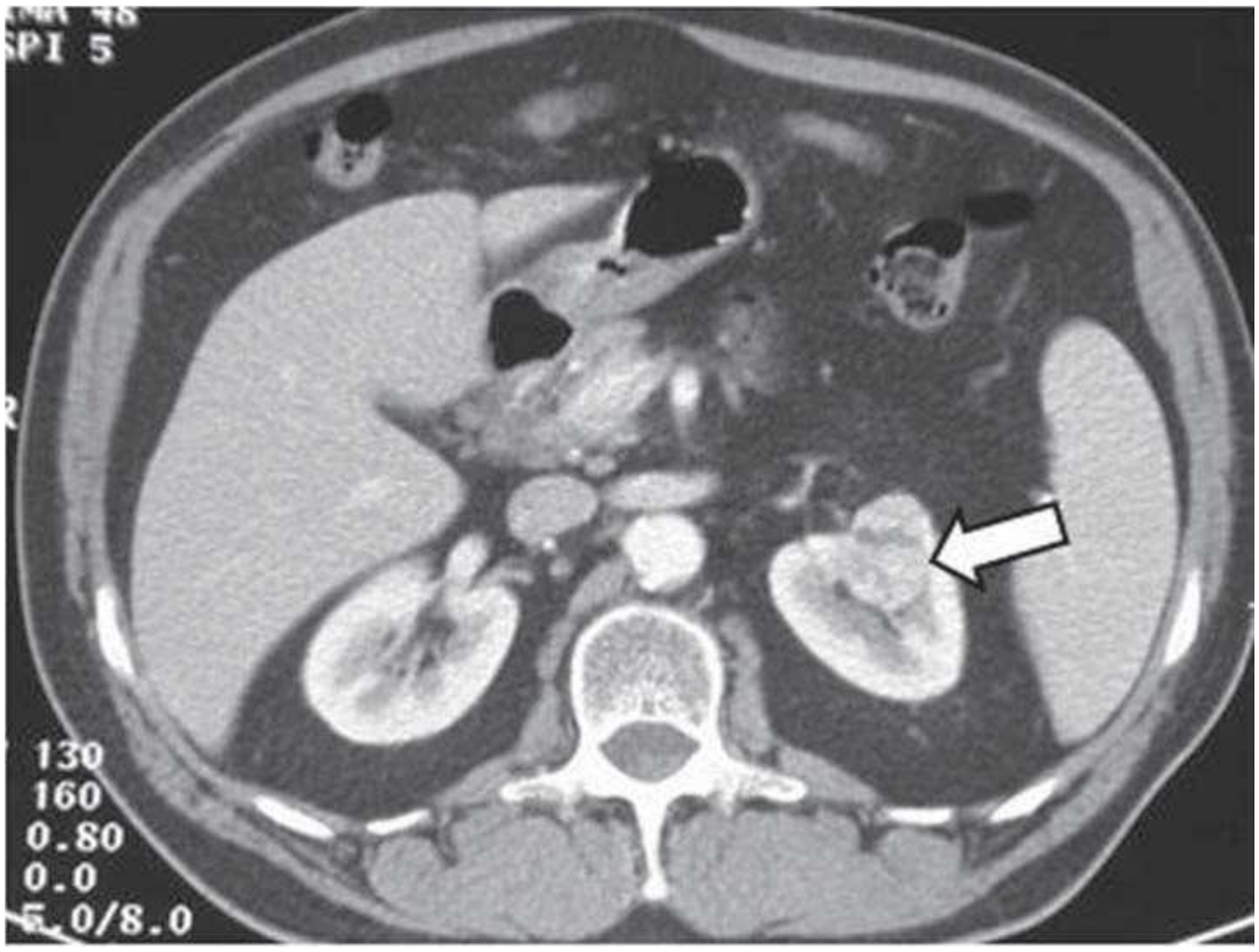

FIGURE 11.25 Contrast-enhanced CT showing a subtle left renal cell cancer replacing the left renal sinus fat.

fat or the adjacent liver, spleen, or paraspinous musculature; an interruption of the perirenal fascial planes, renal veins, and inferior vena cava; and perihilar and perivascular adenopathy can be assessed accurately by CT scans or MRIs. MRIs and CT scans have been shown to be comparable in the diagnosis and the staging of renal cell carcinomas. Because of greater spatial resolution, a CT scan is superior to an MRI in detecting small lesions, and an MRI has not been used as a screening tool in patients with hematuria. However, MRIs have been shown to be more accurate than CT scans in tumor staging. MRIs are particularly beneficial for the evaluation of the patency of the renal veins and inferior vena cava, the delineation of perivascular lymphadenopathy, and the extension of the tumor into adjacent organs.[93,115–117] Three-dimensional image reconstructions of renal tumors can be obtained with MDCT.[56,118] This information can help the surgeon, especially if a partial nephrectomy is being considered. CT-guided radiofrequency ablations of renal cell carcinomas are an alternative treatment option, particularly in patients that are not surgical candidates. CT scans are also used to follow these patients to assess for residual disease or recurrence.[9,40,56,93,102,106,108,119–124] In many institutions, a CT scan is the technique of choice for the diagnosis and staging of renal cell cancer; an MRI is used when a contrast-enhanced CT scan is contraindicated, or if frequent follow-up is required in high-risk patients.[93,115–117]

Renal Lymphoma or Leukemia

Primary lymphoma of the kidney is rare because there is no lymphatic tissue within the kidneys. Renal involvement may be due to hematogenous spread or contiguous invasion from an adjacent retroperitoneal lymphadenopathy. The kidneys are more commonly involved in non-Hodgkin lymphoma than in Hodgkin lymphoma, particularly when the disease has relapsed.[125–127]

Renal lymphoma has a variable radiologic appearance on CT scans and MRIs. The most common pattern is multiple masses that are of the same or slightly higher attenuations than normal renal parenchyma on an unenhanced CT scan and are low to intermediate in signal intensity on T1- and T2-weighted MRIs. Lymphomas are hypovascular tumors and demonstrate lower contrast enhancement than normal renal parenchymas[125–127] on contrast-enhanced CT scans or MRIs

FIGURE 11.26 Contrast-enhanced CT showing a large right renal carcinoma with heterogeneously enhancing solid areas and necrosis.

FIGURE 11.27 Contrast-enhanced CT showing a low-attenuation mass in the left kidney consistent with lymphoma.

(Fig 11.27). Other appearances include a direct invasion from adjacent retroperitoneal lymphadenopathy, an infiltrative pattern with renal enlargement, or a solitary mass.[125–127]

Leukemic renal infiltration is frequently seen at a postmortem examination and can be associated with renal impairment. It may present as unilateral or bilateral renal enlargement or focal mass or masses.[128]

Metastatic Disease

Primary tumors that may metastasize to the kidney include carcinomas of the lung, breast, adrenal gland, and colon; malignant melanoma; and non-Hodgkin lymphoma.[41,43] These tumors may present as either a solitary or multiple focal mass that demonstrates less enhancement than normal renal parenchyma on a contrast-enhanced CT scan or an MRI. The direct extension of extrarenal retroperitoneal tumors may lead to renal obstruction and a loss of function.[41,43]

Renal Sarcomas

Sarcomas of the kidney are rare. They present as solid masses that may grow very large in size and vary in their degree of vascularity.[129] Large tumors often contain central areas of necrosis. The imaging characteristics are nonspecific, making it difficult to distinguish a renal sarcoma from a renal cell carcinoma.

Transitional Cell Carcinoma

Transitional cell carcinomas of the renal collecting system and ureter present with three characteristic appearances on a CT scan or an MRI: sessile soft-tissue filling defects in the lumen of the enhanced collecting system (Fig. 11.28) or ureter; thickening of uroepithelial wall; or infiltrating nonenhancing renal masses (Fig. 11.29). Tumors may be smooth or papillary in contour and may cause ureteral obstruction and renal functional impairment. In addition to assessing the collecting system and ureter, CT urography allows us to detect and characterize renal lesions and extrarenal masses and is more sensitive in detecting renal calculi.[28,32,43,52,54,56,93,130] A CT urography is also the imaging of choice for tumor staging, demonstrating the invasion of perihilar fat and associated lymph node enlargement. Alternatively, an MR urography can be used to assess the collecting system in patients with a contraindication to iodinated contrast CT scans.

Renal Trauma

Renal injury is common, occurring in 8% to 10% of the cases of blunt and penetrating abdominal trauma. About 90% of renal injuries result from blunt force injury and 10% from penetrating

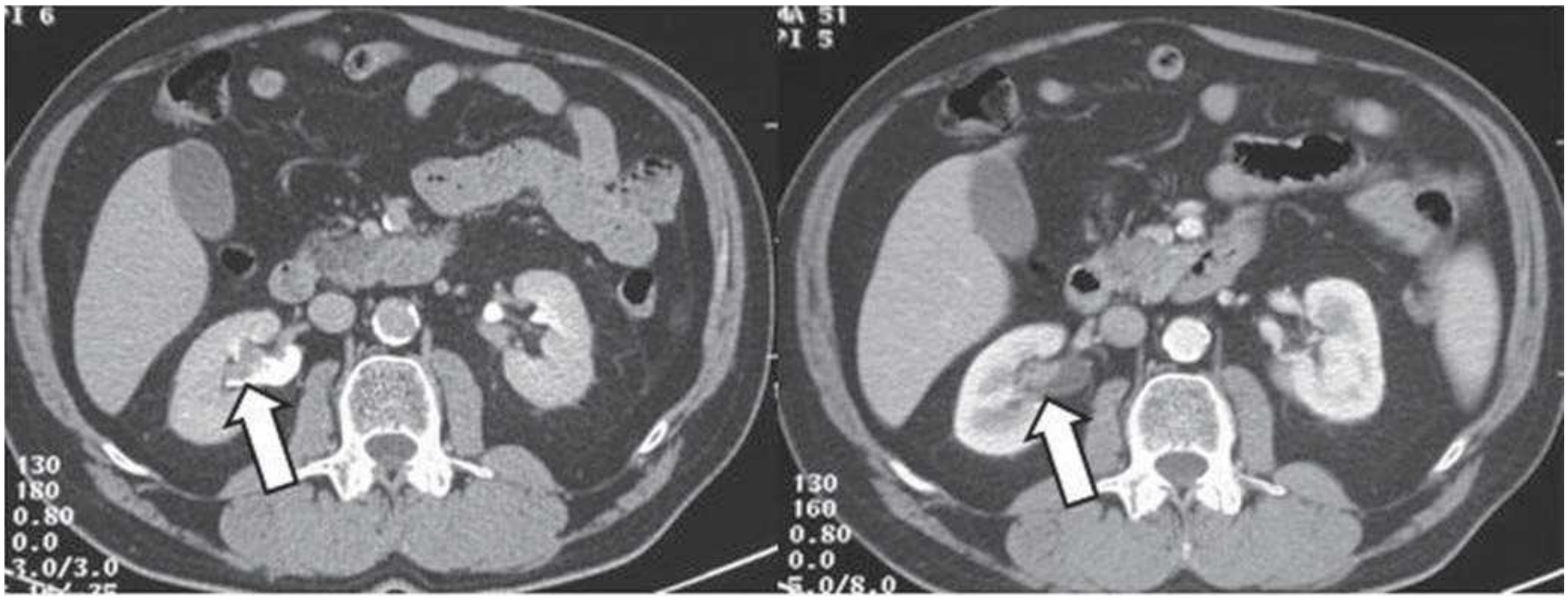

FIGURE 11.28 TCC in right kidney presenting as a filling defect on the excretory phase (*left*) and demonstrating subtle enhancement on an earlier enhancement phase (*right*).

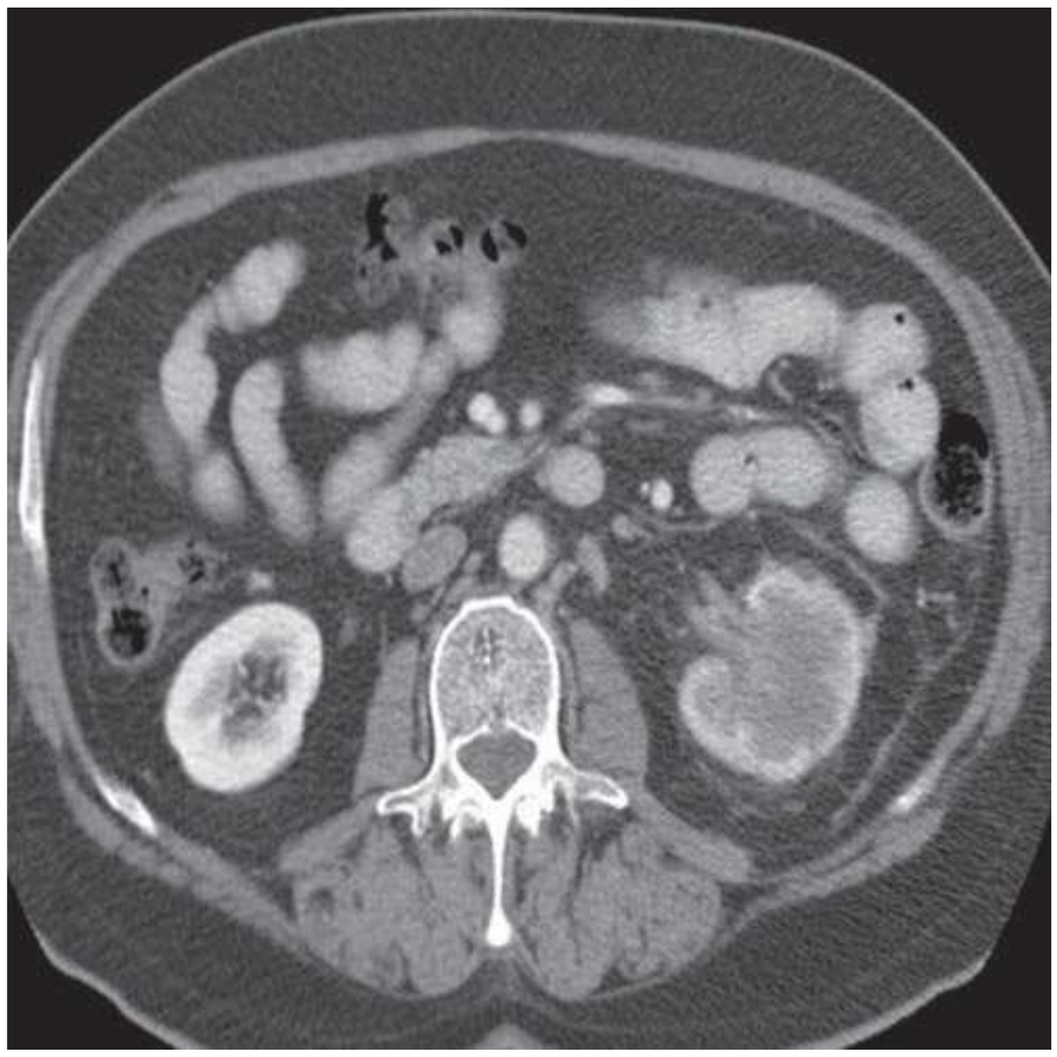

FIGURE 11.29 TCC in left kidney presenting as diffuse infiltrating mass that effaces the normal corticomedullary differentiation, resulting in a faceless kidney.

FIGURE 11.30 Unenhanced CT showing a focal hyperdense area in the right kidney consistent with contusion. Contrast in the collecting system is from contrast-enhanced CT performed a day prior.

trauma, but vary somewhat with location. The clinical indications for the imaging evaluation of the genitourinary system depend on several factors, including the overall hemodynamic status of the patient, other injuries sustained, the site of blunt or penetrating trauma, and the presence or absence of gross hematuria.[37,56,131] The American Association for the Surgery of Trauma (AAST) has devised a renal injury severity score based on surgical observations. A CT grading scale following the surgical management is classified as grade I, a minor contusion with or without concomitant subcapsular hematoma; grade II, a superficial laceration without the involvement of the collecting system; grade III, a deep parenchymal laceration with or without urinary extravasation; and grade IV, a renal pedicle injury.

The majority of blunt renal injuries are CT grades I and II and are managed conservatively without intervention.[37,56,131] Contusions are visualized as ill-defined low attenuation areas with irregular margins in the renal parenchyma. They may appear as regions with a striated nephrogram due to differential blood flow through the contused parenchyma or as focal areas of renal parenchymal extravasation on delayed CT studies (Fig. 11.30). These lesions usually resolve during follow-up imaging.[37,56,131] More significant renal trauma may or may not require intervention by angiography or surgery. Controversy exists over the management of grade III injury, with the most recent trend favoring conservative therapy. Grade IV and penetrating renal injuries are surgically explored.[132–134]

Patients with suspected renal injuries who are clinically stable can benefit greatly from a CT assessment. A contrast enhanced CT scan can detect renal contusions and lacerations. Lacerations present with irregular streaks of low attenuation within the contrast-enhanced renal parenchyma and are classified as incomplete lacerations (affecting the renal parenchyma without communicating with pelvicalyceal structures) and complete lacerations (interrupting the collecting system). Subcapsular hematomas are shown as a lower density intracapsular hemorrhage compressing the enhanced kidney (Fig. 11.31).

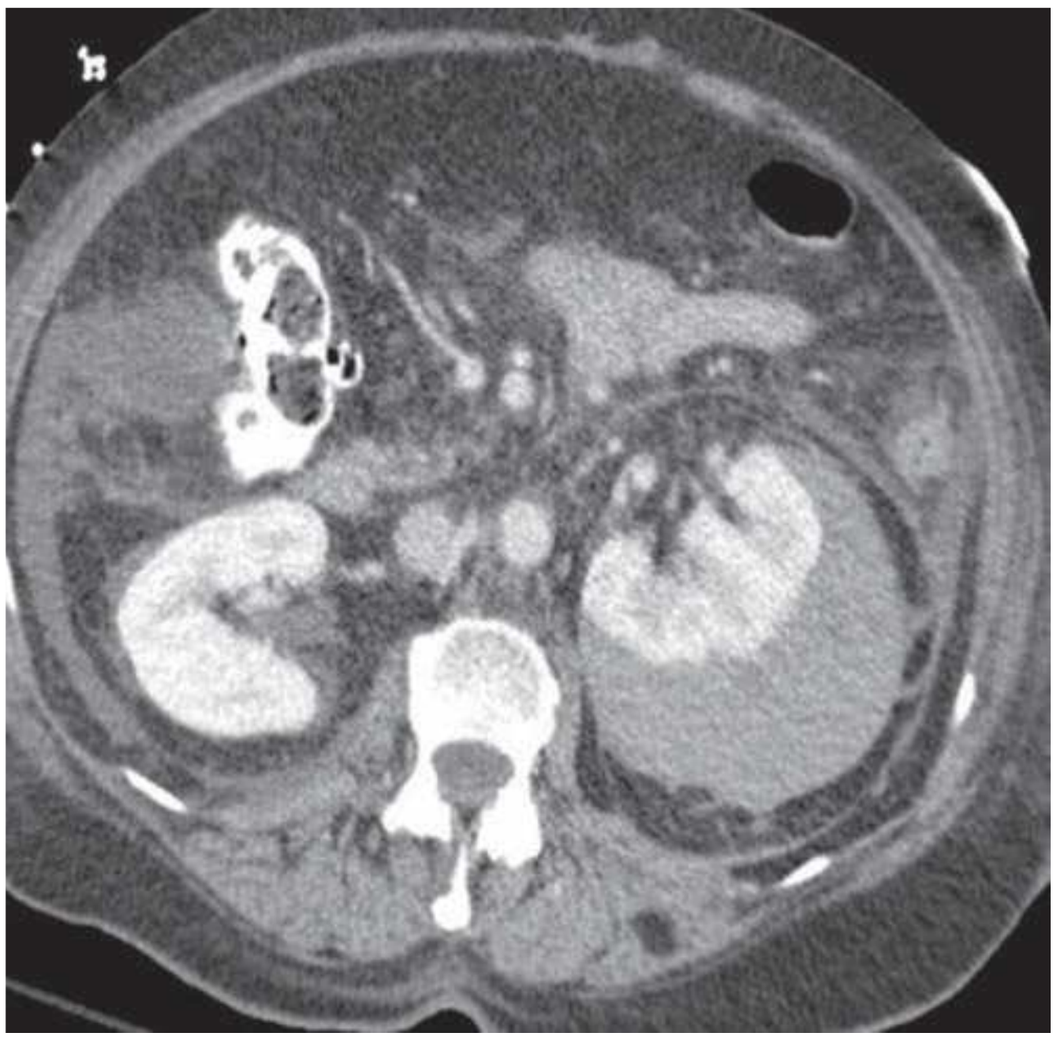

FIGURE 11.31 Contrast-enhanced CT showing a large left subcapsular hematoma displacing the left kidney.

FIGURE 11.32 Contrast-enhanced CT showing shattered left kidney with perirenal hematoma.

Extravasated blood varies in its CT scan attenuation value, depending on the age of the hematoma and the hemoglobin content. With fluid collections filling the perirenal or pararenal spaces and displacing the kidney, a perirenal hemorrhage or urine extravasation (best seen on delayed images) should be considered. Fresh blood may have a higher attenuation value than extravasated urine in an unenhanced CT scan. Renal infarction may occur with a segmental occlusion of polar arteries due to trauma.[132–134] On a CT scan, catastrophic renal injuries, such as shattered kidneys, can be easily detected (Fig. 11.32). Concomitant injuries to other visceral organs may be present.[132–134] When there are underlying renal abnormalities including renal cysts, tumors, and hydronephrosis, relatively minor trauma may result in major injuries to kidneys, thereby confounding the diagnosis.

REFERENCES

1. Hu H. Multi-slice helical CT: scan and reconstruction. Med Phys. 1999;26(1):5–18.
http://www.ncbi.nlm.nih.gov/pubmed/9949393

2. Cody DD. AAPM/RSNA physics tutorial for residents: topics in CT. Image processing in CT. Radiographics . 2002;22(5):1255–1268.
http://www.ncbi.nlm.nih.gov/pubmed/12235351

3. Sheth S, Fishman EK. Multi-detector row CT of the kidneys and urinary tract: techniques and applications in the diagnosis of benign diseases. Radiographics. 2004;24(2):e20.

4. Van Der Molen AJ, Cowan NC, Mueller-Lisse UG, et al. CT urography: definition, indications and techniques. A guideline for clinical practice. Eur Radiol. 2008;18(1):4–17.

5. Townsend BA, Silverman SG, Mortele KJ, et al. Current use of computed tomographic urography: survey of the society of uroradiology. J Comput Assist Tomogr . 2009;33(1):96–100.

6. O'Donoghue PM, McSweeney SE, Jhaveri, K. Genitourinary imaging: current and emerging applications. J Postgrad Med. 2010;56(2):131–139.
http://www.ncbi.nlm.nih.gov/pubmed/20622393

7. Amendola MA. Comparison of MR imaging and CT in the evaluation of renal masses. Crit Rev Diagn Imaging . 1989;29(2):117–150.
http://www.ncbi.nlm.nih.gov/pubmed/2540936

8. Blake MA, Kalra MK. Genitourinary tract imaging. Preface. Radiol Clin North Am . 2008;46(1):xi–xii.

9. Prasad SR, Dalrymple NC, Surabhi VR. Cross-sectional imaging evaluation of renal masses. Radiol Clin North Am . 2008;46(1):95–111, vi–vii.
http://www.ncbi.nlm.nih.gov/pubmed/18328882

10. Bettmann MA. Frequently asked questions: iodinated contrast agents. Radiographics . 2004;24(Suppl 1):S3–S10.

11. Burgener FA, Hamlin DJ. Contrast enhancement in abdominal CT: bolus vs. infusion. AJR Am J Roentgenol . 1981;137(2):351–358.
http://www.ncbi.nlm.nih.gov/pubmed/6789645

12. Bae KT. Intravenous contrast medium administration and scan timing at CT: considerations and approaches. Radiology. 2010;256(1):32–61.

13. Balter S. An introduction to the physics of magnetic resonance imaging. Radiographics. 1987;7(2):371–383.
http://www.ncbi.nlm.nih.gov/pubmed/3448640

14. Goddard P, Jackson P. The physics of magnetic resonance imaging: a simplif ed approach . Bristol Med Chir J. 1988;103(2):7.
http://www.ncbi.nlm.nih.gov/pubmed/3219633

15. Leyendecker JR, Clingan MJ. Magnetic resonance urography update—are we there yet? Semin Ultrasound CT MR. 2009;30(4):246–257.
http://www.ncbi.nlm.nih.gov/pubmed/19711638

16. Chandarana H, Lee VS. Renal functional MRI: are we ready for clinical application? AJR Am J Roentgenol. 2009;192(6):1550–1557.

17. Jacobs MA, Ibrahim TS, Ouwerkerk R. AAPM/RSNA physics tutorials for residents: MR imaging: brief overview and emerging applications. Radiographics . 2007;27(4):1213–1229.

18. Saloner D. The AAPM/RSNA physics tutorial for residents. An introduction to MR angiography. Radiographics. 1995;15(2):453–465.
http://www.ncbi.nlm.nih.gov/pubmed/7761648

19. Cogbill TH, Ziegelbein KJ. Computed tomography, magnetic resonance, and ultrasound imaging: basic principles, glossary of terms, and patient safety. Surg Clin North Am. 2011;91(1):1–14.
http://www.ncbi.nlm.nih.gov/pubmed/21184898

20. Morcos SK, Haylor J. Pathophysiology of nephrogenic systemic f brosis: a review of experimental data. World J Radiol. 2010;2(11):427–433.

21. Perazella MA, Reilly RF. Imaging patients with kidney disease: how do we approach contrast-related toxicity? Am J Med Sci. 2011;341(3):215–221.

22. Kulkarni MV, Shaff MI, Sandler MP, et al. Evaluation of renal masses by MR imaging . J Comput Assist Tomogr. 1984;8(5):861–865.
http://www.ncbi.nlm.nih.gov/pubmed/6088602

23. Pedrosa I, Chou MT, Ngo L, et al. MR classification of renal masses with pathologic correlation. Eur Radiol. 2008;18(2):365–375.
http://www.ncbi.nlm.nih.gov/pubmed/17899106

24. Choyke PL, Hricak H, Kenney PJ, et al. The future of research in genitourinary radiology: through the looking glass—a view from the Society of Uroradiology. Radiology. 1998;207(1):3–6.
http://www.ncbi.nlm.nih.gov/pubmed/9530290

25. Gilfeather M, Woodward PJ. MR imaging of the adrenal glands and kidneys. Semin Ultrasound CT MR. 1998;19(1):53–66.
http://www.ncbi.nlm.nih.gov/pubmed/9503520

26. Kramer LA. Magnetic resonance imaging of renal masses. World J Urol . 1998;16(1):22–28.
http://www.ncbi.nlm.nih.gov/pubmed/9542011

27. Dockery WD, Stolpen AH. State-of-the-art magnetic resonance imaging of the kidneys and upper urinary tract. J Endourol. 1999;13(6):417–423.
http://www.ncbi.nlm.nih.gov/pubmed/10479007

28. Krestin GP. Genitourinary MR: kidneys and adrenal glands. Eur Radiol . 1999;9(9):1705–1714.

29. Goldman SM, Sandler CM. Genitourinary imaging: the past 40 years. Radiology . 2000;215(2):313–324.
http://www.ncbi.nlm.nih.gov/pubmed/10796901

30. Tello R, Davison BD, O'Malley M, et al. MR imaging of renal masses interpreted on CT to be suspicious. AJR Am J Roentgenol. 2000;174(4): 1017–1022.

31. Akbar SA, Shirkhoda A, Jafri SZ. Normal variants and pitfalls in CT of the gastrointestinal and genitourinary tracts. Abdom Imaging . 2003;28(1): 115–128.

32. Herts BR. Imaging for renal tumors. Curr Opin Urol . 2003;13(3):181–186.
http://www.ncbi.nlm.nih.gov/pubmed/12692438

33. Israel GM, Krinsky GA. MR imaging of the kidneys and adrenal glands. Radiol Clin North Am . 2003;41(1):145–159.
http://www.ncbi.nlm.nih.gov/pubmed/12630690

34. Ho VB, Choyke PL. MR evaluation of solid renal masses. Magn Reson Imaging Clin N Am . 2004;12(3):413–427, v.
http://www.ncbi.nlm.nih.gov/pubmed/15271363

35. Bellin MF. [Genitourinary imaging]. J Radiol . 2005;86(7–8):862–863.
http://www.ncbi.nlm.nih.gov/pubmed/16342866

36. Nikken JJ, Krestin GP. MRI of the kidney—state of the art. Eur Radiol . 2007;17(11):2780–2793.
http://www.ncbi.nlm.nih.gov/pubmed/22902039

37. Silverman SG, Leyendecker JR, Amis ES Jr. What is the current role of CT urography and MR urography in the evaluation of the urinary tract? Radiology. 2009;250(2):309–323.
http://www.ncbi.nlm.nih.gov/pubmed/19188307

38. Thornbury JR. Perirenal anatomy: normal and abnormal. Radiol Clin North Am . 1979;17(2):321–331.
http://www.ncbi.nlm.nih.gov/pubmed/472203

39. Korobkin M, Silverman PM, Quint LE, et al. CT of the extraperitoneal space: normal anatomy and fluid collections. AJR Am J Roentgenol .1992;159(5):933–942.
http://www.ncbi.nlm.nih.gov/pubmed/1414803

40. Bechtold RE, Dyer RB, Zagoria RJ, et al. The perirenal space: relationship of pathologic processes to normal retroperitoneal anatomy. Radiographics . 1996;16(4):841–854.

41. Aizenstein RI, Owens C, Sabnis S, et al. The perinephric space and renal fascia: review of normal anatomy, pathology, and pathways of disease spread. Crit Rev Diagn Imaging. 1997;38(4):325–367.
http://www.ncbi.nlm.nih.gov/pubmed/9376088

42. Thornton FJ, Kandiah SS, Monkhouse WS, et al. Helical CT evaluation of the perirenal space and its boundaries: a cadaveric study. Radiology. 2001;218(3):659–663.
http://www.ncbi.nlm.nih.gov/pubmed/11230636

43. Bassignani MJ. Understanding and interpreting MRI of the genitourinary tract. Urol Clin North Am . 2006;33(3):301–317.
http://www.ncbi.nlm.nih.gov/pubmed/16829266

44. Israel GM. MRI of the kidney and urinary tract. J Magn Reson Imaging . 2006;24(4):725–734.

45. Lomas DJ. Optimization of sequences for MRI of the abdomen and pelvis. Clin Radiol . 1997;52(6):412–428.
http://www.ncbi.nlm.nih.gov/pubmed/9202584

46. Schoenberg SO, Knopp MV, Bock M, et al. [MRI of the kidneys. New diagnostic strategies]. Radiologe. 1999;39(5):373–385.

47. Turkvatan A, Olcer T, Cumhur T. Multidetector CT urography of renal fusion anomalies. Diagn Interv Radiol . 2009;15(2):127–134.

48. Niall O, Russell J, MacGregor R, et al., A comparison of noncontrast computerized tomography with excretory urography in the assessment of acute flank pain. J Urol . 1999;161(2):534–537.

49. Borthne A, Pierre-Jerome C, Nordshus T, et al. MR urography in children: current status and future development. Eur Radiol. 2000;10(3):503–511.
http://www.ncbi.nlm.nih.gov/pubmed/10757005

50. Neri E, Boraschi P, Caramella D, et al. MR virtual endoscopy of the upper urinary tract. AJR Am J Roentgenol . 2000;175(6):1697–1702.
http://www.ncbi.nlm.nih.gov/pubmed/11090406

51. Joffe SA, Servaes S, Okon S, et al. Multi-detector row CT urography in the evaluation of hematuria. Radiographics . 2003;23(6):1441–1455; discussion 1455–1456.

52. Kawashima A, Vrtsiska TJ, LeRoy AJ, et al. CT urography. Radiographics. 2004;24 (Suppl 1):S35–S54; discussion S55–S58.

53. McMann LP, Kirsch AJ, Scherz HC, et al. Magnetic resonance urography in the evaluation of prenatally diagnosed hydronephrosis and renal dysgenesis. J Urol. 2006;176(4 Pt 2):1786–1792.

54. Sty JR, Pan CG. Genitourinary imaging techniques. Pediatr Clin North Am. 2006;53(3):339–361, v.
http://www.ncbi.nlm.nih.gov/pubmed/16716784

55. Kajbafzadeh AM, Payabvash S, Sadeghi Z, et al. Comparison of magnetic resonance urography with ultrasound studies in detection of fetal urogenital anomalies. J Pediatr Urol . 2008;4(1):32–39.
http://www.ncbi.nlm.nih.gov/pubmed/18631889

56. O'Connor OJ, McSweeney SE, Maher MM. Imaging of hematuria. Radiol Clin North Am . 2008;46(1):113–132, vii.

57. Smith RC, Verga M, Dalrymple N, et al. Acute ureteral obstruction: value of secondary signs of helical unenhanced CT. AJR Am J Roentgenol . 1996;167(5):1109–1113.

58. Heneghan JP, Dalrymple NC, Verga M, et al. Soft-tissue "rim" sign in the diagnosis of ureteral calculi with use of unenhanced helical CT. Radiology. 1997;202(3):709–711.
http://www.ncbi.nlm.nih.gov/pubmed/9051021

59. Kawashima A, Sandler CM, Boridy IC, et al. Unenhanced helical CT of ureterolithiasis: value of the tissue rim sign. AJR Am J Roentgenol. 1997;168(4): 997–1000.
http://www.ncbi.nlm.nih.gov/pubmed/9124157

60. Bell TV, Fenlon HM, Davison BD, et al. Unenhanced helical CT criteria to differentiate distal ureteral calculi from pelvic phleboliths. Radiology. 1998;207(2):363–367.
http://www.ncbi.nlm.nih.gov/pubmed/9577482

61. Boridy IC, Kawashima A, Goldman SM, et al. Acute ureterolithiasis: nonenhanced helical CT findings of perinephric edema for prediction of degree of ureteral obstruction. Radiology, 1999;213(3):663–667.
http://www.ncbi.nlm.nih.gov/pubmed/10580936

62. Sourtzis S, Thibeau JF, Damry N, et al. Radiologic investigation of renal colic: unenhanced helical CT compared with excretory urography. AJR Am J Roentgenol . 1999;172(6):1491–1494.

63. Dalrymple NC, Casford B, Raiken DP, et al. Pearls and pitfalls in the diagnosis of ureterolithiasis with unenhanced helical CT. Radiographics. 2000;20(2):439–447; quiz 527–528, 532.

64. Soulen MC, Fishman EK, Goldman SM. Sequelae of acute renal infections: CT evaluation. Radiology . 1989;173(2):423–426.
http://www.ncbi.nlm.nih.gov/pubmed/2798873

65. Davidson AJ, Hartman DS, Choyke PL, et al. Radiologic assessment of renal masses: implications for patient care. Radiology . 1997;202(2):297–305.
http://www.ncbi.nlm.nih.gov/pubmed/9015046

66. Rusinek H, Kaur M, Lee VS. Renal magnetic resonance imaging. Curr Opin Nephrol Hypertens . 2004;13(6):667–673.
http://www.ncbi.nlm.nih.gov/pubmed/15483459

67. Mendez G Jr, Isikoff MB, Morillo G. The role of computed tomography in the diagnosis of renal and perirenal abscesses. J Urol . 1979;122(5):582–586.
http://www.ncbi.nlm.nih.gov/pubmed/501808

68. Rodriguez-de-Velasquez A, Yoder IC, Velasquez PA, et al. Imaging the effects of diabetes on the genitourinary system. Radiographics. 1995;15(5):1051–1068.

69. Goldman SM, Hartman DS, Fishman EK, et al. CT of xanthogranulomatous pyelonephritis: radiologic-pathologic correlation. AJR Am J Roentgenol. 1984;142(5):963–969.

70. Israel GM, Bosniak MA. MR imaging of cystic renal masses. Magn Reson Imaging Clin N Am. 2004;12(3):403–412, v.
http://www.ncbi.nlm.nih.gov/pubmed/15271362

71. Israel GM, Hindman N, Bosniak MA. Evaluation of cystic renal masses: comparison of CT and MR imaging by using the Bosniak classification system. Radiology . 2004;231(2):365–371.
http://www.ncbi.nlm.nih.gov/pubmed/15128983

72. Israel GM, Bosniak MA. How I do it: evaluating renal masses. Radiology. 2005;236(2):441–450.
http://www.ncbi.nlm.nih.gov/pubmed/16040900

73. Israel GM, Bosniak MA. Pitfalls in renal mass evaluation and how to avoid them. Radiographics . 2008;28(5):1325–1338.

74. Baumgartner BR, Chezmar JL. Magnetic resonance imaging of the kidneys and adrenal glands. Semin Ultrasound CT MR. 1989;10(1):43–62.
http://www.ncbi.nlm.nih.gov/pubmed/2697325

75. Choyke PL, Filling-Katz MR, Shawker TH, et al. von Hippel- Lindau disease: radiologic screening for visceral manifestations. Radiology. 1990;174(3 Pt 1): 815–820.

76. Hartman DS, Aronson S, Frazer H. Current status of imaging indeterminate renal masses. Radiol Clin North Am. 1991;29(3):475–496.
http://www.ncbi.nlm.nih.gov/pubmed/2024002

77. Semelka RC, Shoenut JP, Kroeker MA, et al. Renal lesions: controlled comparison between CT and 1.5-T MR imaging with nonenhanced and gadolinium-enhanced fat-suppressed spin-echo and breath-hold FLASH techniques. Radiology, 1992;182(2):425–430.
http://www.ncbi.nlm.nih.gov/pubmed/1732961

78. Balci NC, Semelka RC, Patt RH, et al., Complex renal cysts: findings on MR imaging. AJR Am J Roentgenol . 1999;172(6):1495–1500.

79. Higgins JC, Fitzgerald JM. Evaluation of incidental renal and adrenal masses. Am Fam Physician . 2001;63(2):288–294, 299.

80. EL-Merhi FM, Bae KT. Cystic renal disease. Magn Reson Imaging Clin N Am. 2004;12(3):449–467, vi.
http://www.ncbi.nlm.nih.gov/pubmed/15271365

81. Silverman SG, Mortele KJ, Tuncali K, et al. Hyperattenuating renal masses: etiologies, pathogenesis, and imaging evaluation. Radiographics. 2007;27(4):1131–1143.
http://www.ncbi.nlm.nih.gov/pubmed/17620471

82. Ravine D, Gibson RN, Walker RG, et al. Evaluation of ultrasonographic diagnostic criteria for autosomal dominant polycystic kidney disease 1. Lancet . 1994;343(8901):824–827.
http://www.ncbi.nlm.nih.gov/pubmed/7908078

83. Harris PC, Bae KT, Rossett S, et al. Cyst number but not the rate of cystic growth is associated with the mutated gene in autosomal dominant polycystic kidney disease. J Am Soc Nephrol. 2006;17(11):3013–3019.

84. Nascimento AB, Mitchell DG, Zhang XM, et al. Rapid MR imaging detection of renal cysts: age-based standards. Radiology, 2001;221(3):628–632.
http://www.ncbi.nlm.nih.gov/pubmed/11719656

85. Bae KT, Grantham JJ. Imaging for the prognosis of autosomal dominant polycystic kidney disease. Nat Rev Nephrol. 2010;6(2):96–106.
http://www.ncbi.nlm.nih.gov/pubmed/20111050

86. Torres VE, Granthan JJ, Chapman AB, et al. Potentially modifiable factors affecting the progression of autosomal dominant polycystic kidney disease. Clin J Am Soc Nephrol. 2011;6(3):640–647.
http://www.ncbi.nlm.nih.gov/pubmed/21088290

87. Taylor AJ, Cohen EP, Erickson SJ, et al. Renal imaging in long-term dialysis patients: a comparison of CT and sonography. AJR Am J Roentgenol. 1989;153(4):765–767.

88. Choyke PL. Acquired cystic kidney disease. Eur Radiol . 2000;10(11): 1716–1721.
http://www.ncbi.nlm.nih.gov/pubmed/11097395

89. Levine E, Grantham JJ, Slusher SL, et al. CT of acquired cystic kidney disease and renal tumors in long-term dialysis patients. AJR Am J Roentgenol. 1984;142(1):125–131.

90. Takebayashi S, Ono Y, Sakai F, et al. Computed tomography of amyloidosis involving retroperitoneal lymph nodes mimicking lymphoma. J Comput Assist Tomogr . 1984;8(5):1025–1027.

91. Schoth F, Persigehl T, Palmowski M. Current role and future perspective of MRI for diagnosis and characterization of renal cell carcinoma. Panminerva Med. 2010;52(4):307–318.
http://www.ncbi.nlm.nih.gov/pubmed/21183891

92. Lang EK. Angio-computed tomography and dynamic computed tomography in staging of renal cell carcinoma. Radiology . 1984;151(1):149–155.
http://www.ncbi.nlm.nih.gov/pubmed/6701305

93. Aslaksen A, Gothlin JH. Imaging of solid renal masses. Curr Opin Radiol . 1991;3(5):654–662.
http://www.ncbi.nlm.nih.gov/pubmed/1931501

94. Krestin GP. Magnetic resonance imaging of the kidneys: current status. Magn Reson Q . 1994;10(1):2–21.

95. Papachristopoulos G, Bis KG, Shetty AN, et al. Breath-hold 3D MR angiography of the renal vasculature using a contrast-enhanced multiecho gradient-echo technique. Invest Radiol . 1999;34(12):731–738.

96. Israel GM, Lee VS, Edye M, et al. Comprehensive MR imaging in the preoperative evaluation of living donor candidates for laparoscopic nephrectomy: initial experience. Radiology . 2002;225(2):427–432.
http://www.ncbi.nlm.nih.gov/pubmed/12409576

97. Kawamoto S, Montgomery RA, Lawler LP, et al. Multidetector CT angiography for preoperative evaluation of living laparoscopic kidney donors. AJR Am J Roentgenol. 2003;180(6):1633–1638.
http://www.ncbi.nlm.nih.gov/pubmed/12760934

98. Raman SS, Pojchamarnwiputh S, Muangsomboon K, et al. Surgically relevant normal and variant renal parenchymal and vascular anatomy in preoperative 16-MDCT evaluation of potential laparoscopic renal donors. AJR Am J Roentgenol. 2007;188(1):105–114.
http://www.ncbi.nlm.nih.gov/pubmed/17179352

99. Hohenwalter MD, Skowlund CJ, Erickson SJ, et al., Renal transplant evaluation with MR angiography and MR imaging. Radiographics . 2001;21(6): 1505–1517.

100. Akbar SA, Jafri SZ, Amendola MA, et al. Complications of renal transplantation. Radiographics . 2005;25(5):1335–1356.
http://www.ncbi.nlm.nih.gov/pubmed/16160115

101. Marotti M, Hricak H, Fritzsche P, et al. Complex and simple renal cysts: comparative evaluation with MR imaging. Radiology . 1987;162(3):679–684.
http://www.ncbi.nlm.nih.gov/pubmed/3809481

102. Eilenberg SS, Lee JK, Brown J, et al. Renal masses: evaluation with gradient-echo Gd-DTPA-enhanced dynamic MR imaging. Radiology. 1990;176(2): 333–338.

103. Semelka RC, Hricak H, Stevens SK, et al. Combined gadolinium-enhanced and fat-saturation MR imaging of renal masses. Radiology. 1991;178(3): 803–809.

104. Rominger MB, Kenney PJ, Morgan DE, et al. Gadolinium-enhanced MR imaging of renal masses. Radiographics. 1992;12(6):1097–1116; discussion 1117–1118.
http://www.ncbi.nlm.nih.gov/pubmed/1439014

105. Kawashima A, Goldman SM, Sandler CM. The indeterminate renal mass. Radiol Clin North Am . 1996;34(5):997–1015.
http://www.ncbi.nlm.nih.gov/pubmed/8784393

106. Kreft BP, Müller-Miny H, Sommer T, et al. Diagnostic value of MR imaging in comparison to CT in the detection and differential diagnosis of renal masses: ROC analysis. Eur Radiol . 1997;7(4):542–547.
http://www.ncbi.nlm.nih.gov/pubmed/9204336

107. Wagner BJ. The kidney: radiologic-pathologic correlation. Magn Reson Imaging Clin N Am. 1997;5(1):13–28.
http://www.ncbi.nlm.nih.gov/pubmed/8995122

108. Sheth S, Scatarige JC, Horton KM, et al. Current concepts in the diagnosis and management of renal cell carcinoma: role of multidetector CT and three-dimensional CT. Radiographics . 2001;21:S237–S254.

109. Zandrino F, Rescinito G, Calabrese M, et al. Pictorial essay: magnetic resonance imaging of adrenal masses. Radiol Med. 2002;103(3):206–218.
http://www.ncbi.nlm.nih.gov/pubmed/11976617

110. Burdeny DA, Semelka RC, Kelekis NL, et al. Small (< 1.5 cm) angiomyolipomas of the kidney: characterization by the combined use of in-phase and fat-attenuated MR techniques. Magn Reson Imaging. 1997;15(2):141–145.

111. Castagnetti M, Vezzù, Leverda A, et al. Urological counseling and followup in pediatric tuberous sclerosis complex. J Urol . 2007;178(5):2155–2159.
http://www.ncbi.nlm.nih.gov/pubmed/17870119

112. Israel GM, Hindman N, Hecht E, et al. The use of opposed-phase chemical shift MRI in the diagnosis of renal angiomyolipomas. AJR Am J Roentgenol . 2005;184(6):1868–1872.
http://www.ncbi.nlm.nih.gov/pubmed/15908544

113. Kim JI, Cho JY, Moon KC, et al. Segmental enhancement inversion at biphasic multidetector CT: characteristic finding of small renal oncocytoma. Radiology . 2009;252(2):441–448.
http://www.ncbi.nlm.nih.gov/pubmed/19508984

114. Li G, Cuilleron M, Gentil-Perret A, et al. Characteristics of image-detected solid renal masses: implication for optimal treatment. Int J Urol . 2004;11(2):63–67.
http://www.ncbi.nlm.nih.gov/pubmed/14706008

115. Zhang J, Israel GM, Krinsky GA, et al. Masses and pseudomasses of the kidney: imaging spectrum on MR. J Comput Assist Tomogr. 2004;28(5):588–595.
http://www.ncbi.nlm.nih.gov/pubmed/15480030

116. Roy C, Sauer B, Lindner V, et al. MR Imaging of papillary renal neoplasms: potential application for characterization of small renal masses. Eur Radiol. 2007;17(1):193–200.

117. Pedrosa I, Sun MR, Spencer M, et al. MR imaging of renal masses: correlation with findings at surgery and pathologic analysis. Radiographics. 2008;28(4):985–1003.
http://www.ncbi.nlm.nih.gov/pubmed/18635625

118. Kalra MK, Maher MM, D'Souza R, et al. Multidetector computed tomography technology: current status and emerging developments. J Comput Assist Tomogr . 2004;28(Suppl 1):S2–S6.

119. Lang EK. Comparison of dynamic and conventional computed tomography, angiography, and ultrasonography in the staging of renal cell carcinoma. Cancer . 1984;54(10):2205–2214.
http://www.ncbi.nlm.nih.gov/pubmed/6386140

120. Peppercorn PD, Phillips RR, Webb JA, et al. Rapid MRI assessment of renal space-occupying lesions. Eur Radiol . 2000;10(4):579–582.
http://www.ncbi.nlm.nih.gov/pubmed/10795536
121. Delgado Dominguez E. [MR in renal masses]. Arch Esp Urol .2001;54(6):583–592.
122. Hélénon O, André M, Correas JM, et al. [Characterization of renal masses]. J Radiol . 2002;83(6 Pt 2):787–804.
123. Farrell MA, et al. Imaging-guided radiofrequency ablation of solid renal tumors. AJR Am J Roentgenol . 2003;180(6):1509–1513.
124. Israel GM, Bosniak MA. Renal imaging for diagnosis and staging of renal cell carcinoma. Urol Clin North Am . 2003;30(3):499–514.
http://www.ncbi.nlm.nih.gov/pubmed/12953751
125. Eisenberg PJ, Papanicolaeou N, Lee MJ, et al. Diagnostic imaging in the evaluation of renal lymphoma. Leuk Lymphoma . 1994;16(1–2):37–50.
126. Imai Y, Sone S, Serizawa S, et al. [Magnetic resonance imaging of renal lymphoma with computed tomography correlation]. Nippon Igaku Hoshasen Gakkai Zasshi. 1995;55(8):562–568.
127. Semelka RC, Kelekis NL, Burdeny DA, et al. Renal lymphoma: demonstration by MR imaging. AJR Am J Roentgenol. 1996;166(4):823–827.
http://www.ncbi.nlm.nih.gov/pubmed/8610558
128. Pickhardt PJ, Lonergan GJ, Davis CJ Jr, et al. From the archives of the AFIP. Infiltrative renal lesions: radiologic-pathologic correlation. Armed Forces Institute of Pathology. Radiographics. 2000;20(1):215–243.
http://www.ncbi.nlm.nih.gov/pubmed/10682782
129. Agrons GA, Kingsman KD, Wagner BJ, et al. Rhabdoid tumor of the kidney in children: a comparative study of 21 cases. AJR Am J Roentgenol. 1997;168(2):447–451.
http://www.ncbi.nlm.nih.gov/pubmed/9016225
130. Roy C. [MRI of the urinary tract: recent developments and future applications]. J Radiol . 2004;85(2 Pt 2):171–183.
http://www.ncbi.nlm.nih.gov/pubmed/15094608
131. Ramchandani P, Buckler PM. Imaging of genitourinary trauma. AJR Am J Roentgenol . 2009;192(6):1514–1523.
http://www.ncbi.nlm.nih.gov/pubmed/19457813
132. Becker CD, Mentha G, Schmidlin F, et al. Blunt abdominal trauma in adults: role of CT in the diagnosis and management of visceral injuries. Part 2: gastrointestinal tract and retroperitoneal organs. Eur Radiol . 1998;8(5): 772–780.
http://www.ncbi.nlm.nih.gov/pubmed/9601964
133. Porter JM, Singh T. Value of computed tomography in the evaluation of retroperitoneal organ injury in blunt abdominal trauma. Am J Emerg Med . 1998;16(3):225–227.
http://www.ncbi.nlm.nih.gov/pubmed/9596419
134. Daly KP, Ho CP, Persson DL, et al. Traumatic retroperitoneal injuries: review of multidetector CT findings. Radiographics. 2008;28(6):1571–1590.
http://www.ncbi.nlm.nih.gov/pubmed/18936022